Bulletin of Volcanology (2025) 87:63
https://doi.org/10.1007/s00445-025-01848-7

RESEARCH ARTICLE

Zircon ages and compositions record Quaternary magma mingling and plutonic-volcanic links on Ascension Island, South Atlantic

Jane H. Scarrow[1] · Katy J. Chamberlain[2] · Pilar Montero[1] · Matthew S. A. Horstwood[3] · Jenni Barclay[4]

Received: 3 March 2025 / Accepted: 14 June 2025 / Published online: 9 July 2025

Abstract

Isolated ocean islands pose challenges for managing volcanic hazards because of their remote locations. Some, such as Ascension Island in the South Atlantic, have diverse hazards associated with variable magmatic compositions and eruptive styles, as evidenced by past volcanic deposits. In this context, zircon ages and compositions provide insights into the timing and nature of magma generation, storage, and eruption. Specifically, zircon crystallisation ages record magmatic cyclicity. This study examines zircon growth in a small ocean island context, focusing on juvenile volcanic pumice-scoria and plutonic clasts from the only known explosive deposit on island showing evidence of mingling between mafic and felsic magmas. Dating reveals a U-Th-Pb crystallisation age for the "Mingled Fall" juvenile components of $0.60+0.11/-0.17$ Ma (MSWD = 0.92). However, recycling of rocks and crystals from older magmatic events, at ~ 0.9 Ma and ~ 1.3 Ma, is recorded in both volcanic deposits and plutonic clasts within these. Hafnium (εHf 2.75–13.77) and oxygen ($\delta^{18}O$ 4.3–6.54‰) isotopic analyses point, respectively, to melting of a moderately enriched mantle source and pre-mingling assimilation of hydrothermally altered crustal rocks. These data support explosive eruption triggered by mingling of mantle-derived mafic magma with rhyolitic magma from partially melted gabbroic lower crust. Furthermore, varying zircon Ce and Eu anomalies indicate a transition in the magmatic system redox state from reducing to oxidising as crystallisation progressed. We also highlight the underexploited potential of U-Th-Pb SHRIMP analysis to date zircon in young Quaternary volcanic rocks, providing a valuable tool for hazard assessment and monitoring.

Keywords Pleistocene · U-Th-Pb dating · Ocean island volcanism · Rhyolite-basalt · Granite-monzonite-syenite

Introduction

Hazards related to ocean island volcanism include explosive and effusive eruptions, earthquakes, gases, landslides and tsunamis that pose a range of associated risks for vulnerable local populations. To mitigate the impacts of such hazards effectively, it is essential to understand the causes and evolution of past eruptions, to anticipate the style and composition of future events. However, despite an overall increase in analysis and interpretation of zircon ages and compositions in recent years, this mineral is still currently rarely used in studies of recent and active volcanic systems. Geochronological and compositional data from zircon, which is often preserved through successive magmatic cycles as a result of its chemical and physical resilience, can provide insights into eruptive processes (Hanchar and Hoskin 2003). In particular, light is shed on the following: cyclicity of crystallisation and eruption ages (e.g., Marsden et al. 2021a; Scarrow et al. 2021; Rojas-Agramonte et al. 2022; Famin et al. 2022; Schmitt et al. 2023); primary mantle source characteristics (e.g., Xu et al. 2018; Sagan et al. 2020); tectonomagmatic context and provenance (e.g., Grimes et al. 2015; Coutts et al. 2019; Friedrichs et al. 2020); assimilation, fractionation and hydrothermal processes (e.g., Carley et al. 2011;

Editorial responsibility: R. Sulpizio

✉ Jane H. Scarrow
jscarrow@ugr.es

[1] Department of Mineralogy and Petrology, Faculty of Sciences, University of Granada, 18071 Granada, Spain

[2] Department of Earth, Ocean and Ecological Sciences, University of Liverpool, 4 Brownlow Street, Liverpool L69 3GP, UK

[3] British Geological Survey, Nicker Hill, Keyworth, Nottingham NG12 5GG, UK

[4] School of Earth Sciences, University of Bristol, Wills Memorial Building, Queens Road, Bristol BS8 1RJ, UK

Bindeman et al. 2012; Troch et al. 2018; Cisneros de León and Schmitt 2019; Scarrow et al. 2022); thermobarometry (Loucks et al. 2020; Ni et al. 2020); and magma volumes (e.g., Weber et al. 2020). So, insights preserved within zircon can elucidate magma source characteristics and interactions (Scarrow et al 2023). Here, we use zircon data to consider the petrogenetic processes that generated both end member magmas and their degree of interaction, as well as associated plutonic clasts in the only known mingled fall on Ascension Island in the South Atlantic. Such deposits are, however, evident on other ocean islands, for example in the Canaries and the Azores, where the mixed characteristics of mingled deposits, e.g., textures, inclusion types and zoning, provide critical insights into the dynamics of magma mixing, the structure and zonation of a magmatic plumbing system and how these systems evolve over time (Freundt and Schminke 1992). Evidence of short-lived interactions between compositionally distinct magmas, such as basanite and phonolite, highlight the potential for genetically unrelated magmas to interact (Wiesmaier et al. 2011; Araña et al. 1994), which can shed light on how intrusions, convection and volatile exsolution destabilise and trigger explosive eruptions (Laeger et al. 2019). For example, rapid magma mixing processes driven by bubble-enhanced turbulence revealed the structure, dynamics and explosivity of the Tajogaite 2021, La Palma, volcanic plumbing system (González-García et al. 2023). We specifically consider the duration of the magmatic system and the role of magmatic and eruptive processes in mineral recycling between different reservoirs and distinct events.

Ascension Island crustal structure is conditioned by subsurface plutonism (Chamberlain et al. 2019) which places an important control on the passage of magma to the surface and, therefore, the closed-system fractional crystallisation of small-volume magma batches (Kar et al. 1998; Jicha et al. 2013). The oceanic crust beneath the island is sampled by accidental lithic clasts preserved in the volcanic deposits (e.g., Scarrow et al. 2023) which can provide rare insights into plutonism in the region (cf., Shane et al. 2012) and consequently the pathways by which evolved melt reservoirs are generated and preserved. Notably, closed system fractional crystallisation modelling of the trachybasalt mafic scoria end member from the only known macroscopic-scale preservation of magma mingling on the island, the Mingled Fall, could not reproduce the most evolved pumice composition, felsic rhyolite (Chamberlain et al. 2020), at depths of crystallisation consistent with melt inclusion volatiles and major elements. The rhyolites could be modelled, however, by ~ 10% partial melting of lower crustal olivine-rich gabbros which produced the evolved magma (Chamberlain et al. 2020; cf., Sigurdsson 1977; Hildreth 1981; Kimura and Hayasaka 2019; Angelo 2013). Intrusion of water-rich, originally crystal-poor, mafic magma apparently triggered devolatilisation of the water-rich rhyolitic magma leading to ascent of the mingled magma with heterogeneous compositions and viscosities (Chamberlain et al. 2020). We analysed zircon compositions and ages from all components of the Mingled Fall to investigate these processes further.

This work focuses on zircon U-Th-Pb ages of the volcanic deposits and plutonic accidental lithic clasts from the Mingled Fall. The precise age of crystallisation and eruption of the Mingled Fall deposit was unknown, but its relative stratigraphy constrained because it crops out between a pumice breccia dated at 0.693 ± 0.047 Ma and a 0.591 ± 0.017 Ma pumice (Ar/Ar dating, Preece et al. 2021). Our new accessory mineral age and compositional data can be integrated into existing stratigraphic and volcanological frameworks (Chamberlain et al. 2020; Preece et al. 2021). This allows us to place further constraints on the timing of processes in the magmatic system as well as providing specific insights into the following: tectonomagmatic context; assimilation; melt generation; crystallisation and fractionation; hydrothermal processes; thermobarometry; eruption and the identification of marker horizons for tephrostratigraphic correlations (cf., Hanchar and Hoskin 2003; Schmitt et al. 2006; Grimes et al. 2015; Danišík et al. 2017; Troch et al. 2018; Xu et al. 2018; Loucks et al. 2020; Friedrichs et al. 2021; Marsden et al. 2021a, 2021b; Sturm et al. 2024).

Here, we integrate field information and macrocryst phase data (Chamberlain et al. 2020) with new fieldwork results, whole-rock compositions and zircon U-Th-Pb ages and isotopic and trace element data from both juvenile (pumice and scoria) and accidental plutonic clasts from the Mingled Fall deposit. This approach enables us to constrain petrogenetic processes, characterise magma sources and unravel magmatic cyclicity. In addition, controls are placed on pre-eruptive plumbing processes that led to mineral recycling between different reservoirs and magmatic events, ultimately resulting in explosive eruption.

Geological setting, field relations and petrological context

Ascension Island is a small mid-Atlantic volcanic island, located at 7°56′S, 14°22′W, ~ 50 km south of the Ascension fracture zone and 100 km west of the Mid-Atlantic Ridge (Fig. 1, inset). It is part of the British Overseas Territory that also comprises Saint Helena and Tristan da Cunha and serves as a crucial hub for British and American military bases, ships and aircraft, as well as being a base for vital communication infrastructure. The resident population of ~ 1000 includes military personnel. The subaerial volcanic edifice, with dimensions of 8 km by 12 km, preserves the last 1 Myr of the 5–6 Ma volcanism (Kar et al. 1998; Klingelhöfer et al. 2001; Paulick et al. 2010; Jicha et al. 2013; Preece et al. 2016). Magmatism has

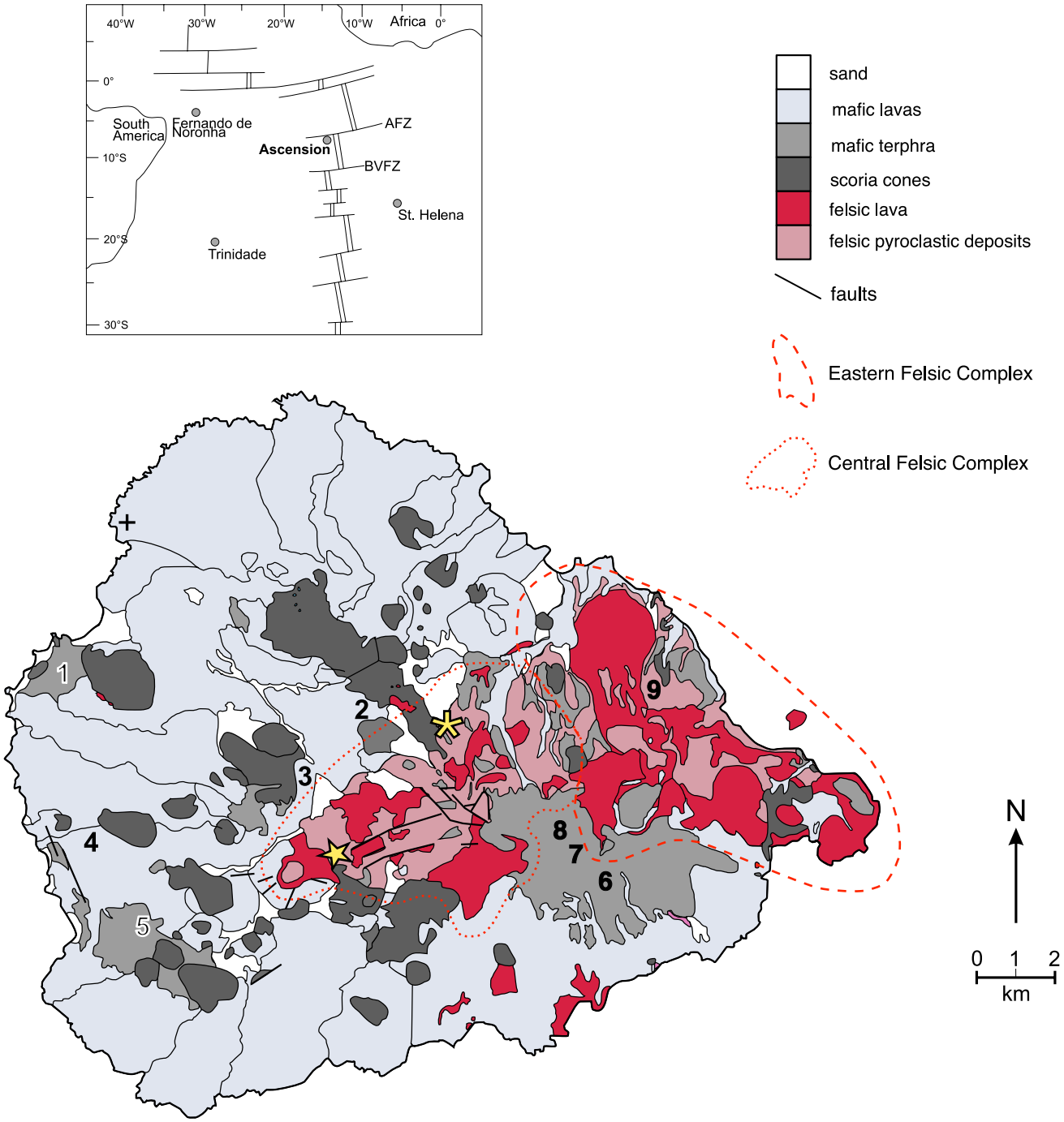

Fig. 1 Simplified geological map of Ascension Island adapted from (Chamberlain et al. 2016) showing the distribution of mafic and felsic effusive and explosive products, and locations of key infrastructure and outcrops. 1, Georgetown; 2, Two Boats Village; 3, Royal Air Force Station, Travelers Hill; 4, USA Military Base; 5, Wideawake aerodrome; 6, NASA road; 7, Middleton Ridge; 8, Green Mountain; 9, Echo Canyon. A yellow asterisk marks the location of the Debris Avalanche (DA) outcrop of the Mingled Fall deposit, a yellow star marks the Middleton Ridge (MR) outcrop and a black cross the youngest basaltic lava flows. Inset: Ascension Island relative to the Mid-Atlantic Ridge in the South Atlantic, Ascension Fracture Zone (AFZ) and Boca Verde Fracture Zone (BVFZ)

been related to melting of an anomalously enriched Mid-Atlantic Ridge-type mantle displaced by westward plate movement (Paulick et al. 2010) or an off-centre deflected shallow, low-flow mantle plume (Gaherty & Dunn 2007). The growth of the volcanic edifice has overthickened the crust by up to 12 km (Klingelhöfer et al. 2001; Minshull et al. 2010). This crustal structure permitted differentiation of mantle-derived melts by varying degrees of fractional

crystallisation, mineral segregation and accumulation during stalling and ascent (Kar et al. 1998; Chamberlain et al. 2016, 2019). The broad compositional range of Ascension Island volcanic rocks resulted, comprising a silica-undersaturated transitional to mildly alkaline series of basalt–hawaiite–mugearite–benmoreite–trachyte–rhyolite (Daly 1925; Weaver et al. 1996). Mafic-felsic plutonic and volcanic accidental lithic clasts (Harris 1986; Kar et al. 1998; Scarrow et al. 2023) identified in juvenile volcanic material mainly crop out in explosive pyroclastic deposits rather than effusive flows and domes (Weaver et al. 1996; Chamberlain et al. 2020; Davies 2021).

The Mingled Fall mafic scoria and felsic pumice deposit is variably preserved in outcrops across the Central Felsic Complex of the island, with particularly complete sequences at Middleton Ridge and in the Debris Avalanche Area (Fig. 1, star and asterisk, respectively). A detailed description of the volcanic stratigraphy of the Mingled Fall can be found in Chamberlain et al. (2020). Figure 2 shows the complete sequence, from base to top with no evidence, such as paleosols, for breaks in the sequence: a basal thin (< 10 cm) white ash (A), overlain by two thin (< 20 cm) upward-coarsening well-sorted, dense, scoria units (L1); well-sorted mixed (to varying degrees) dense light grey and

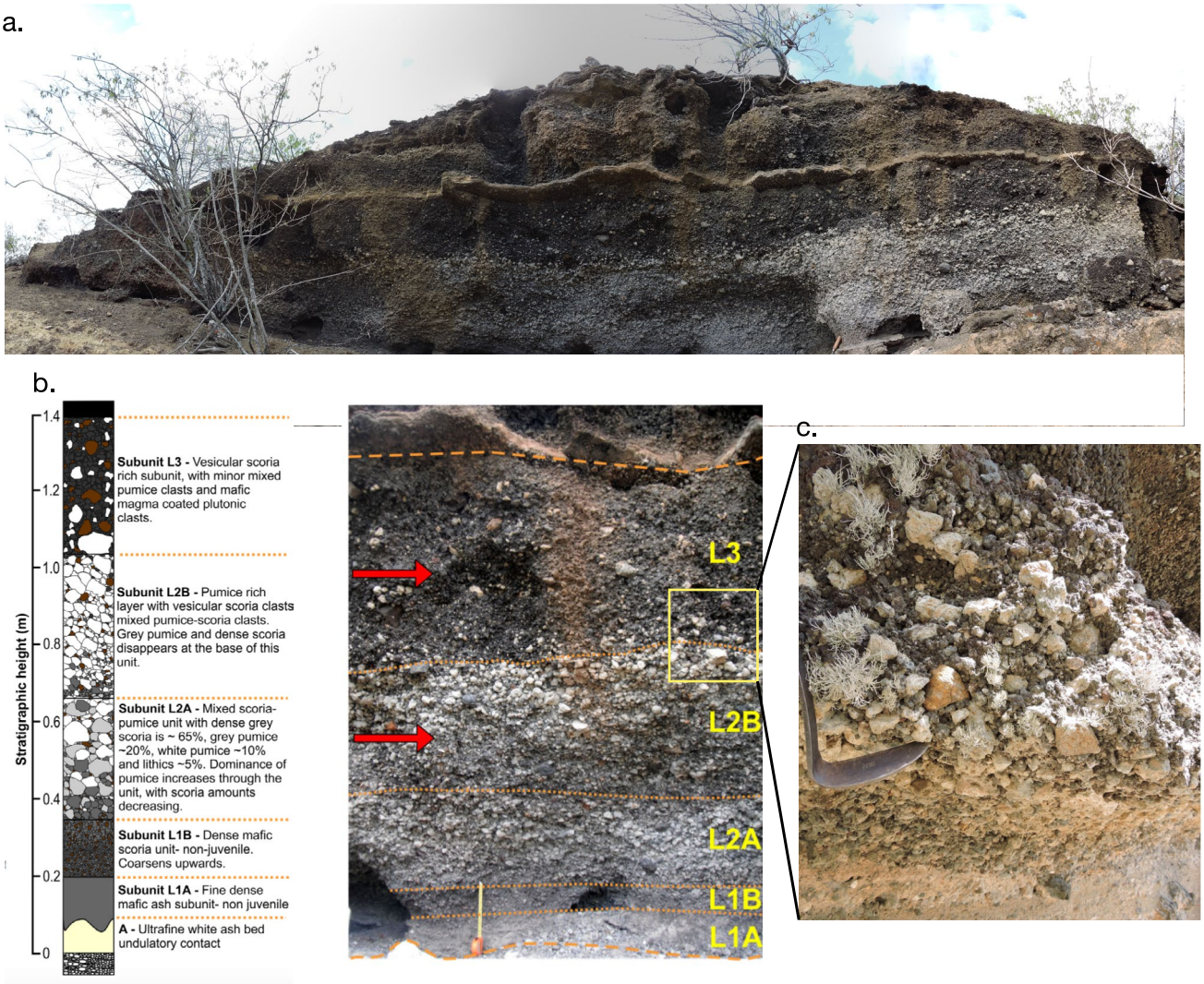

Fig. 2 (**a**) "Debris Avalanche" outcrop of the Mingled Fall. Note the progression from light-coloured pumice at the base to dark scoria at the top of the outcrop. Plutonic accidental lithic clasts are concentrated in the central scoria unit. The outcrop is 1.5 m high. This mingled deposit crops out across the Central Felsic Complex (Fig. 1) where the oldest subaerial rocks of Ascension Island are located. The positions of some of the samples taken from the outcrop are marked in yellow (see Supplementary Material Table 1 for information about the samples studied). (**b**) Stratigraphy of the Mingled Fall, from Chamberlain et al. (2020), red arrows indicate typical pumice and scoria sampling locations. There is no evidence of a temporary break, such as a paleosol or an erosion surface between the units. (**c**) Close up of the unit L2B to L3 transition, note the plutonic clast in the centre of the image, tool blade 10 cm

very vesicular white pumice units with individual clasts mingled with scoria (L2); well-sorted scoria with rare mingled pumice clasts as well as abundant monzonitic–granitic–syenitic plutonic and rare basaltic and rhyolitic accidental lithic clasts (L3). The pumice blocks are angular with a glassy groundmass and well-developed vesicularity, whereas the scoria clasts are dense and sub-rounded with limited vesicularity (Chamberlain et al. 2020). In addition to the distinct pumice and scoria clasts, some individual pieces show evidence of mingling, e.g., small mafic blebs within the pumice and felsic glass in the scoria.

Published mineral data (Chamberlain et al. 2020) from juvenile samples of the Mingled Fall show pumice olivine is fayalite; clinopyroxene is Na-rich with elevated Sc, Zn, Sr, Zr, Y; and feldspars are unzoned anorthoclase with low concentrations of Zn, Sr, Ba, Eu, and Pb. By contrast, the scoria feldspars are also unzoned but more compositionally diverse from orthoclase to labradorite with higher, more scattered Zn, Sr, Ba, Eu, and Pb values; clinopyroxene is Na-poor with high Ti and Co; and olivine is more forsteritic ($Fa_{47–54}$) than in the pumice. Mineral chemistry data from Harris (1982, without stratigraphic context) indicates the plutonic accidental lithic clast mineral compositions are quite varied: andesine to albite feldspars with zoning from more Na-rich cores to more K-rich rims; augite-aegirine some of which are Ti–rich; edenite to arfvedsonite and rare aenigmatite amphibole; and almost pure fayalitic olivine is also present in a few blocks.

Analysing melt inclusions in olivine and clinopyroxene phenocrysts and the glass selvedge rims on these Chamberlain et al. (2020) measured up to 8.28 wt% H_2O in the pumice and 6.04 wt% in the scoria. Using the MagmaSat application (Ghiorso and Gualda 2015), they calculated entrapment pressures of 330 MPa, ~ 11 km, for both the scoria- and pumice-hosted rhyolitic melt inclusions. Correlating these with geophysical data, this corresponds with the base of the oceanic crust, ~ 1 km above the seismic Moho (Klingelhöfer et al. 2001). Eruption of the gabbro-melt-generated rhyolites was triggered by mafic hydrous mantle magma (Chamberlain et al. 2020). These authors concluded that the felsic melt in the melt inclusions represents the most evolved end member of the Mingled Fall mixed magma. This interacted variably with the mafic end member to produce the pumice and other, intermediate, compositions.

Samples and methods

Eight representative samples from the same mingled eruptive unit, cropping out at Middleton Ridge (MR) and in the Debris Avalanche Area (DAD) (Fig. 1), were selected for detailed study. These include four juvenile bulk samples: two scorias (861 DAD and 863B MR) and two pumices (606A DAD and 863A MR); and four felsic accidental lithic plutonic clasts—one monzonite (862A7 DAD), one granite (616A MR) and two quartz syenites (862AZ DAD and 616B MR). On the basis of field evidence that indicates the two outcrops are from the same deposit (see Supplementary Material Table 1), we consider the two scoria samples together and the two pumice samples jointly; however, all plutonic accidental lithic clasts were considered individually. Volcanic samples comprise composites of clasts collected from uniform horizontal layers; the decimetre-scale accidental lithic plutonic clasts were excavated from unit L3 (Fig. 2). Petrographic thin sections were made of all samples. Remaining material was prepared for geochemical analyses and zircon separation. All eight samples were powdered for whole-rock major element X-ray fluorescence analysis in a tungsten-carbide ring mill at the University of East Anglia, UK; for elements with concentrations > 0.5 wt%, analyses of multiple international standards yielded uncertainties ≤ ± 0.5 wt% (2σ), except for SiO_2 which yielded uncertainties of ± 1.06 wt% (2σ). Major element data are plotted normalised to 100 wt% dry totals. Rare earth elements plus selected trace elements were analysed by ICP-MS at the University of Granada, Spain, Scientific Facilities Centre (UGR-CIC); precision, as determined from international standards, was better than ± 2% and ± 5% for concentrations of 50 and 5 ppm, respectively.

Zircon was extracted from the eight samples by crushing, sieving using disposable synthetic mesh, then panning the 50–250-μm fraction in water to concentrate heavy minerals. This concentrate was refined by magnetic separation and dissolution of other silicates and phosphates with a mixture of hydrochloric and hydrofluoric acid before hand picking using a binocular microscope. Grains were mounted in epoxy, polished, coated with carbon and then imaged using a Zeiss EVO-150 scanning electron microscope (SEM) at the UGR-CIC. The SEM contrast and brightness settings were constant for all cathodoluminescence analyses permitting comparison of relative intensities between samples. The zircon analytical sequence used was as follows: U-Th-Pb analyses were performed first, then the mount was re-polished until the U–Pb spots disappeared; oxygen isotopes were then analysed on the same grains and in areas close to the previous U-Th-Pb spots, same domain, when possible; trace element analyses were later carried out by LA-ICP-MS on the same areas; finally, Hf isotope analyses were performed on the dated zircon grains.

Zircon was analysed for U-Th-Pb in all eight samples and oxygen isotopes in five samples (two scorias, 861 and 863B; one pumice, 863A; and two accidental plutonic lithic clasts, 862A7 and 862AZ) using the IBERSIMS SHRIMP IIe/mc ion microprobe at the UGR-CIC. All age uncertainties are quoted at 1σ in the text; 1σ errors are plotted for clarity. The 207-corrected ages were calculated by projecting each analytical point from the present-day common lead composition

($^{207}Pb/^{206}Pb \approx 0.85$) onto the Tera-Wasserburg concordia. The current Pb composition is assumed to be the same for all Paleozoic and younger zircons. Also, the effect of ^{230}Th on the $^{206}Pb/^{238}U$ ages was taken into account for young rocks (Schärer 1984). Corrections were proposed by Sakata et al. (2013), implemented by Williams et al. (2016), and used extensively then onwards, e.g., by Rojas-Agramonte et al. (2017). The U/Th ratios used to correct the ^{230}Th effect on the $^{206}Pb/^{238}U$ ages were determined by ICP-MS at the UGR-CIC on a separate aliquot of the same whole-rock samples from which the analysed zircon grains were separated. Zircon U–Pb ratios were analysed by SHRIMP II-Mc following the method described by Williams and Claesson (1987): Each selected spot was rastered with the primary beam for 120 s prior to analysis and then analysed for six scans, following the isotope peak sequence $^{196}Zr_2O$, ^{204}Pb, $^{204.1}$background, ^{206}Pb, ^{207}Pb, ^{208}Pb, ^{238}U, ^{248}ThO and ^{254}UO. Every peak of every scan was measured sequentially 10 times. The counting times per scan for masses 204, 206, 207 and 208 were increased in this case, because of the young age of the zircons, from the standard counting times of 15 s up to 25 s for masses 204, 206, 207 and 208. All calibration procedures were performed on standards included on the same mount: mass calibration REG zircon, ca. 2.5 Ga, very high U, Th and common lead content; SL13 zircon, 563 ± 5 Ma, which is used as a concentration standard, 238 ppm U; and the TEMORA-II zircon, 416.8 ± 1.1 Ma, used as an isotope ratios standard, measured every 4 unknowns. See the Supplementary Material file 'zircon analytical methods' for full SHRIMP analytical details.

It is worth noting that the ages presented here are the youngest zircon dated by the University of Granada IBER-SIMS laboratory and some of the youngest volcanic rocks dated by SHRIMP zircon U-Th-Pb. Although comparable dates include a $^{206}Pb/^{238}U$ zircon age of 0.659 ± 0.044 Ma for the Yellowstone caldera Lava Creek rhyolite tuff (Bindeman et al. 2001) and weighted mean $^{206}Pb/^{238}U$ ages for zircon cores, 0.6599 ± 0.0055 Ma, and rims, 0.6266 ± 0.0058 Ma, for the same rocks (Matthews et al. 2015). Significantly, these young U–Pb ages were measured on a reverse geometry SHRIMP instrument at Menlo Park, CA, USA. The youngest published $^{206}Pb/^{238}U$ zircon age measured on a standard geometry SHRIMP machine was 0.97 ± 0.41 Ma for a southeast Asian mantle-derived zircon megacrysts from Pailin which was supported by LA-ICPMS grain mapping that yielded 1.017 ± 0.067 Ma age (Kirkland et al. 2020).

Once analysed for U-Th-Pb, the megamounts were cleaned, re-polished to erode the pits produced during geochronology analysis and coated with a 30-nm-thick gold layer for oxygen isotope analyses, performed on the IBER-SIMS SHRIMP IIe/mc ion microprobe. Zircon trace element concentrations were analysed at the CIC-UGR LA-ICP-MS laboratory using a PerkinElmer NexION 350X ICP-MS coupled to a New Wave Research NR 213 LA system. Laser ablation Hf isotopes were determined at the British Geological Survey, Keyworth, UK (6 samples: one scoria, 861; two pumices, 606A and 863A; and three lithic clasts 862A7, 862AZ, 616B) using a Thermo-Scientific Neptune Plus MC-ICP-MS. For full details of analytical methods, see Supplementary Material 'zircon analytical methods' file. Complete data sets of whole-rock major and trace elements and zircon U–Th–Pb, O and Hf isotopes and trace element data are given in Supplementary Material Tables 2 and 3.

Results

Whole-rock petrography and composition

Interaction between scoria and pumice is observed in the volcanic deposit of all the Mingled Fall outcrops. Scorias—samples 861 and 863B—are aphanitic, mesocratic, hypohyaline, with a fine-grained inequigranular porphyritic, highly, albeit variably, vesicular texture (40–50 modal% rounded vesicles) (Fig. 3a, b). Macrocrysts, ~ 5–10 modal%, are predominantly subhedral, variably concentrically zoned, plagioclase, up to 1 mm diameter, with minor olivine, clinopyroxene, biotite and Fe-Ti oxides. The groundmass is glassy. Zircon is an accessory mineral. Secondary minerals include rare iddingsite after olivine. Fragments of mm-scale plutonic and volcanic accidental lithic clasts with sharp margins are present in both samples.

Pumices—samples 606A and 863A—are aphanitic, leucocratic, hypohyaline, with a fine-grained inequigranular porphyritic, vesicular texture (30–40 modal%, generally rounded although occasionally elongated vesicles) (Fig. 3c, d). Macrocrysts, comprise ~ 5 modal% subhedral alkali feldspar, up to 1 mm diameter, and minor rounded olivine, clinopyroxene, quartz and Fe-Ti oxides. Zircon and apatite are accessory minerals. Fragments of mm-scale plutonic accidental lithic clasts with disaggregated margins are present in both samples.

Plutonic accidental lithic clasts—862A7, 862AZ, and 616B—are monzonite and quartz syenites with phaneritic, leucocratic-mesocratic, holocrystalline, fine-medium-grained, inequigranular, hypidiomorphic textures and variable development of a late-stage interstitial agpaitic-like mosaic of ferromagnesian minerals (Fig. 3e, f). The mineral assemblage consists of up to 4 mm diameter euhedral plagioclase (~ 70 modal%), alkali feldspar, anhedral interstitial quartz (~ 5–10 modal%) and subhedral-anhedral amphibole, biotite, and Fe-Ti oxides which, in places, form mm-scale patchy polymineralic clusters; olivine and clinopyroxene are present in the monzonite. Zircon and apatite are accessory minerals. Secondary minerals include iddingsite after olivine.

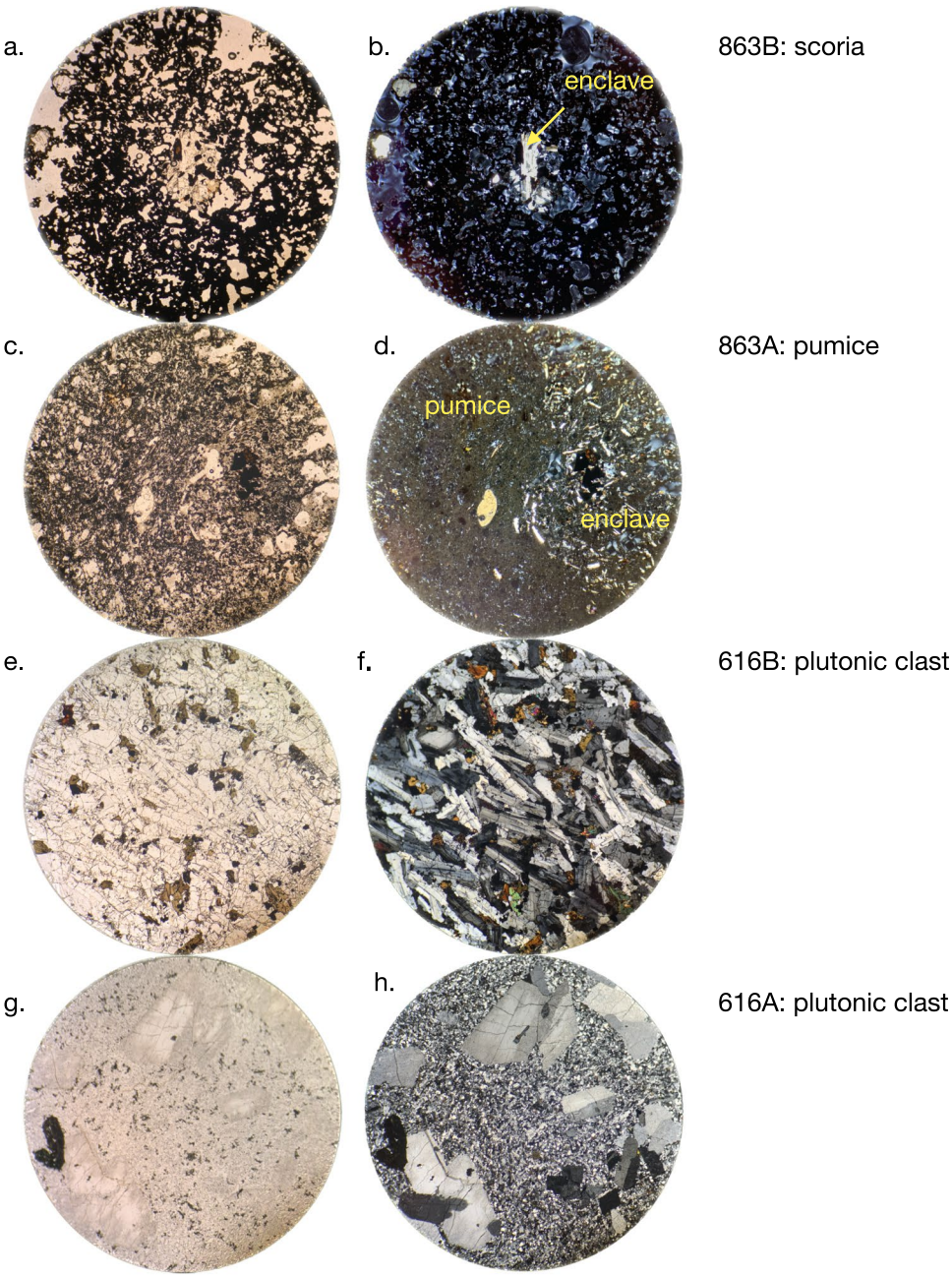

Fig. 3 Photomicrographs of representative samples: **a, b** scoria; **c, d** pumice; and **e, h** plutonic accidental lithic clasts. Fields of view 5.5 mm diameter, polarised light in left-hand column, crossed polars in the right-hand column. K-feld, alkali feldspar; amph, amphibole

Plutonic accidental lithic clast—616A—is a leucocratic peralkaline granite that has a holocrystalline, inequigranular, hypidiomorphic texture with an agpaitic-like mosaic of ferromagnesian minerals (Fig. 3g, h). The mineral assemblage consists of ~ 20 modal% of up to 3 mm subhedral, perthitic, alkali felspar and quartz macrocrysts in a fine-grained feldspar-quartz mosaic. Mafic minerals include dark green amphibole and rare biotite. Zircon and abundant apatite are accessory minerals. Secondary minerals include sericite after feldspar. Glomerocrysts of felsic minerals and mm-scale crustal xenoliths are common.

Whole-rock major and trace element data for the scoria, pumices and plutonic lithic clasts are given in Fig. 4 and Supplementary Material Table 2. Whole-rock compositions for other analysed pumice samples of the same rock types that extend the compositional range are also included in Fig. 4 (Chamberlain et al. 2020 and references therein). For ease of comparison, all analyses are presented and calculated to 100 wt% dry.

All the rocks have an alkaline-transitional metaluminous character (SiO_2 51.94–73.97 wt%; Na_2O+K_2O 5.24–9.41 wt%) with a narrow range of FeOT/MgO (2.95–3.96). The scorias are

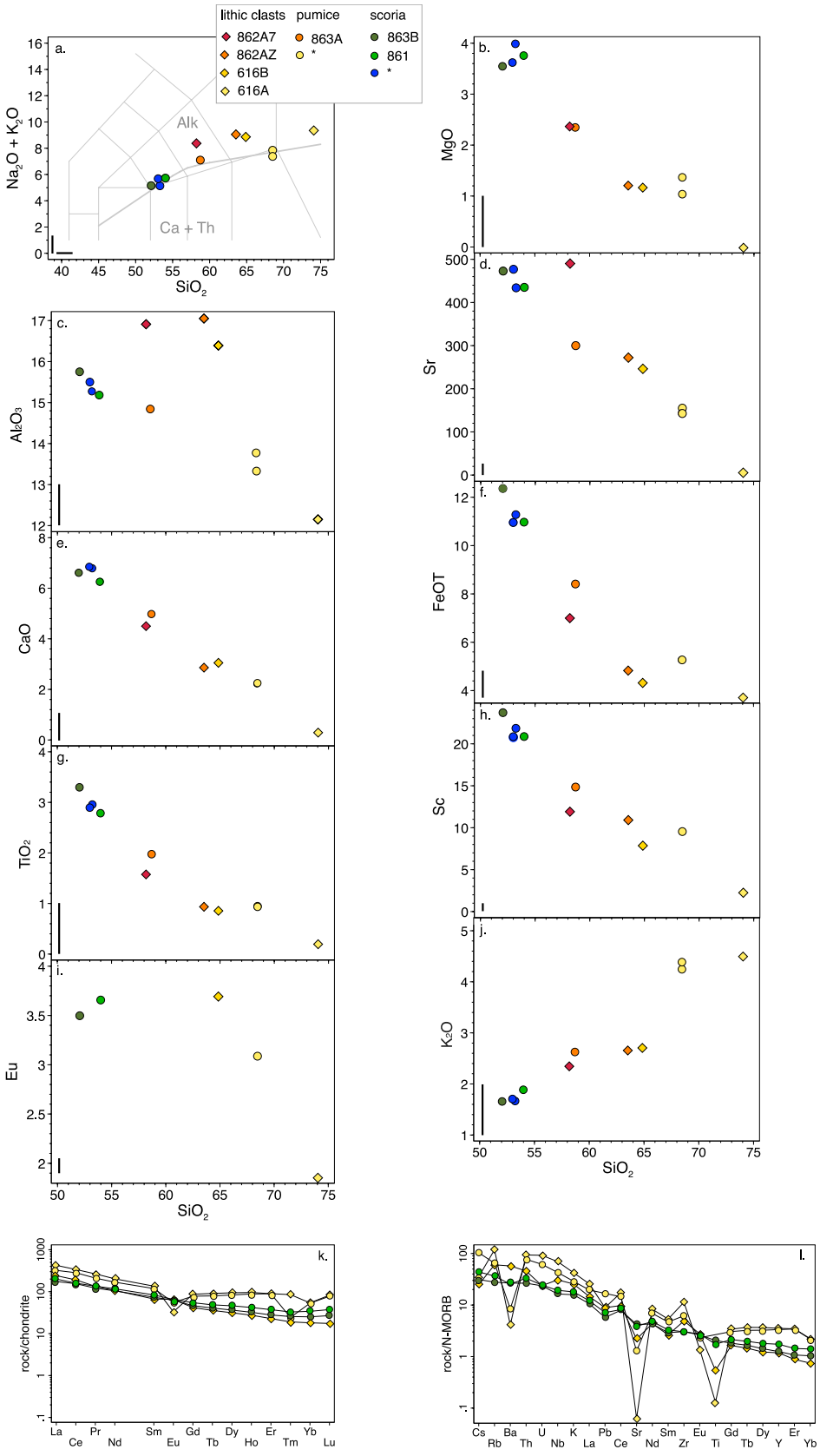

Fig. 4 Whole-rock major and trace elements; major elements are expressed in weight percentage, trace elements in ppm, errors greater than symbol size are shown as a black line in the bottom left corner of the graphs. Major and trace elements vs. SiO_2. **a** $Na_2O + K_2O$; **b** MgO; **c** Al_2O_3; **d** Sr; **e** CaO; **f** FeOT; **g** TiO_2; **h** Sc; **i** Eu; **j** K_2O; **k** Rare Earth diagrams normalised to chondrite (values from Hofmann 1988); and **l** N-MORB (values from McDonough & Sun 1995). *Whole-rock compositions for other analysed pumice samples of the same rock types that extend the compositional range are also included in this figure (cf. Chamberlain et al. 2020 and references therein). For ease of comparison, all analyses are presented and calculated to 100 wt% dry

basaltic trachyandesites; SiO_2 ranges from 51.94 to 53.87 wt% with additional analyses from Chamberlain et al. (2020), extending this to 58.70 wt% SiO_2. The pumice, on the other hand, is a trachyandesite with SiO_2 58.58 wt%, indicating an overlap between the two groups consistent with field observations. This raises the question of whether the compositional overlap results from mingling between a more evolved and a mafic component. Although we prepared our samples by visually selecting the macroscopically least mingled material, potential microscale heterogeneity cannot be ruled out. Supporting this interpretation, pumice analysed by Chamberlain et al. (2020) has a more evolved composition, with trachytes reaching up to 68.35 wt% SiO_2 and pumice- and scoria-hosted melt inclusions as well as matrix glass in both the pumice and scoria being rhyolitic. Although pumice sample 606A was not analysed for major elements, the trace element compositions, such as Rb, Ba, Y and La, indicate it is more evolved than pumice 863A (Supplementary Material Table 2). The monzonite–granite–syenite plutonic accidental lithic clasts range from 58.11 to 73.97 wt% SiO_2. A negative correlation with SiO_2 is observed for most major and trace elements including MgO, FeOT, Al_2O_3, CaO, TiO_2 and P_2O_5 as well as V, Sc and Eu; only K_2O, Sr, Zr and the rare earth elements (REE) show positive correlations with SiO_2 (Fig. 4, Supplementary Material Table 2).

The Mingled Fall juvenile samples all have whole-rock Zr/Hf values of 38 to 42, within the chondritic range, i.e. ~ 35–40, for most crustal rocks (Supplementary Material Table 2, Ahrens and Erlank 1969; Hoskin and Schaltegger 2003). By contrast, all the plutonic accidental lithic clasts have lower, ~ 25, whole-rock Zr/Hf, indicative of fractionation of zircon or other Zr-bearing major phases. Normalised to chondrite, the rocks are slightly enriched in light rare earth elements (LREE) relative to heavy rare earth elements (HREE), $(La/Yb)_N = 5.8–13.3$ (Fig. 4k). The least evolved, lowest SiO_2 scoria and one plutonic clasts show either no Eu anomaly or a slightly positive one, Eu/Eu* = 1.0–1.2 (where Eu = EuN and $Eu^* = \sqrt{[Sm \times Gd]_N}$), whereas the more evolved, higher SiO_2 pumice and plutonic clast have clear negative Eu anomalies, Eu/Eu* = 0.3–0.6, and flatter more elevated middle-heavy REE patterns. Normalised to N-MORB, all the rocks have similar profiles (Fig. 4l): scoria profiles are generally flat and parallel with comparable concentrations, weak negative anomalies are observed in Pb and Sr and in one sample in Ba and Ti relative to adjacent elements; the more-evolved pumice and plutonic clasts have broadly parallel patterns with marked negative anomalies in Ba, Sr and Ti relative to neighbouring elements.

Zircon texture, composition and geochronology

Texture

Representative cathodoluminescence (CL) zircon images from the eight studied samples are presented in Fig. 5. The zircon grains in all samples are texturally diverse with diameters between 50 to 300 µm, equidimensional to prismatic forms and some well-developed pyramidal terminations. Although some cathodoluminescence images suggest the presence of cores and rims, geochronological analyses showed no age difference between internal zones, texturally similar to inherited cores, and external rim zones.

Composition

Trace elements The Mingled Fall zircon REE concentrations vary considerably, within single rock samples; zircon LREE concentrations vary by up to two orders of magnitude and HREE concentrations by less than an order of magnitude (Fig. 6a–g). This variation is consistent with typical intra-grain and inter-grain compositional variations in other magmatic zircon (cf. Hoskin and Schaltegger 2003). The range is greatest in the volcanic samples, scoria sample 861 is most heterogeneous, with less variation in the plutonic clasts. Nevertheless, all plutonic and volcanic zircon chondrite-normalised REE patterns are parallel-subparallel and have similar, typically magmatic, depletion in LREE relative to HREE ($[Gd/Yb]_N$ 0.02–0.12) and positive Ce and negative Eu anomalies relative to adjacent REE (cf. Hoskin and Schaltegger 2003) (Fig. 6).

In the data set as a whole, the zircon Eu anomalies are moderately to strongly negative, Eu/Eu* (0.1–0.6), ($Eu = Eu_N$ and $Eu^* = [Sm \times Gd]_N^{0.5}$), consistent with plagioclase fractionation under reducing conditions before zircon crystallisation (Fig. 6a–g). Notably, the anomalies are parallel in all samples except scoria 861 (and one grain in the plutonic clast 862AZ). The Eu anomalies are comparable to whole-rock data for the most evolved pumice and accidental lithic clasts but not to the less evolved whole-rock compositions in which Eu anomalies are absent or weakly positive (Fig. 4k). However, the prominent negative Eu/Eu* ratios do not correlate systematically with Zr/Hf, a magma differentiation index that reflects preferential melt depletion in Zr relative to slightly less compatible Hf as zircon fractionates (Claiborne et al. 2006). For this reason, the lowest values of Zr/Hf are expected in the most evolved melts that have lower Zr and higher Hf.

A very broad range is evident in zircon Zr/Hf ratios, 19–70, with considerable overlap for all samples; the values are as follows: scoria 861 (62.8–42.5); pumices 606A (55.35–47.6) and 863A (62.6–50.6); and plutonic blocks 616B (53), 862A7 (67.8—27.9) and 862AZ (59.3—32.4). The only correlation with this differentiation index is a positive relation with Ti, in the samples: pumice 606A, scoria 861 and plutonic accidental lithic clast 862A7 (Fig. 6h).

The zircon Ce anomalies are positive, Ce/Ce* (4.4–264, where Ce = Ce and Ce* = [La × Pr]0.5) indicative of oxidising conditions in the magmatic system (Fig. 6a–g). The Ce

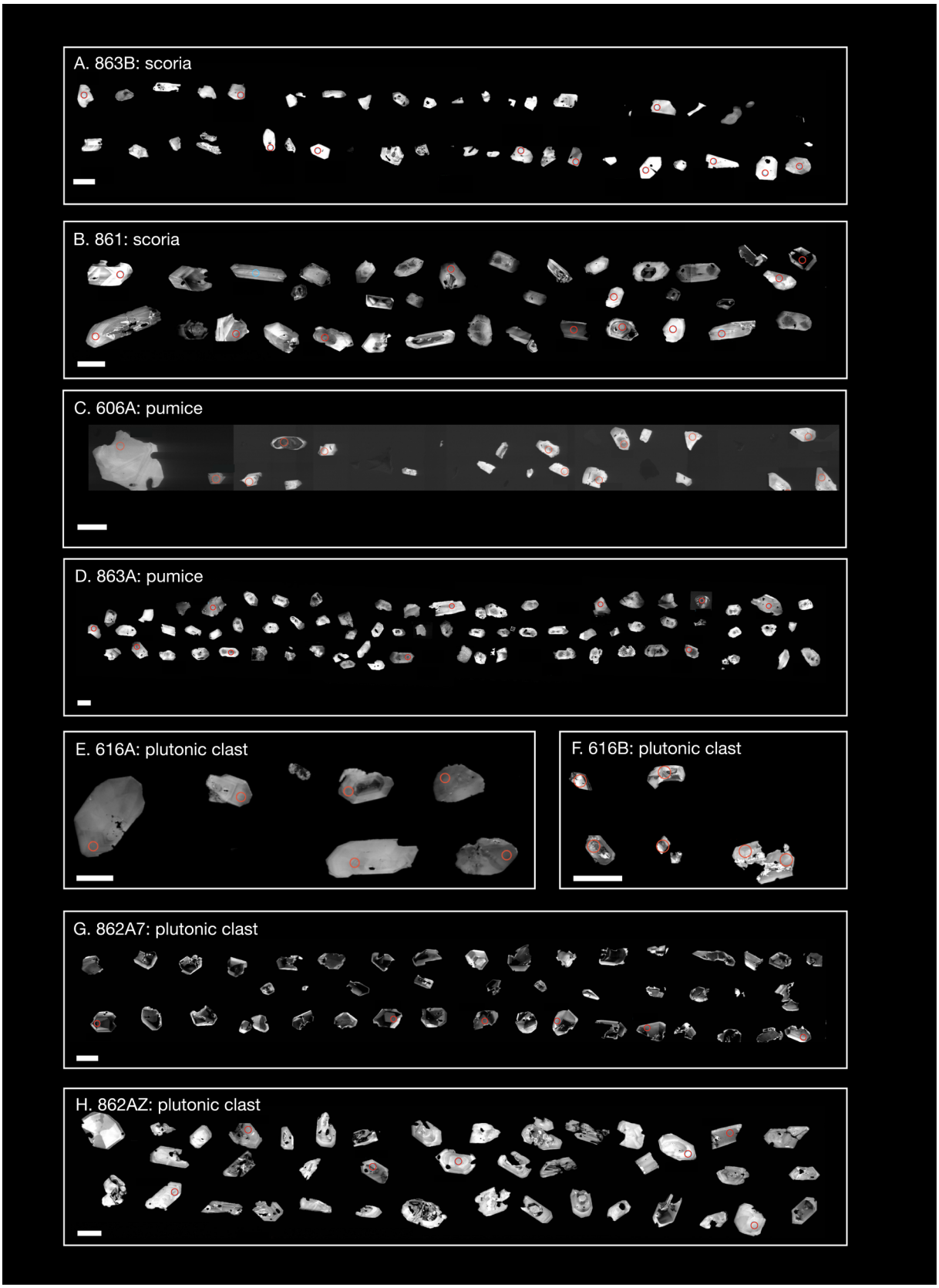

Fig. 5 Representative zircon cathodoluminescence (CL) images of the studied samples. On each image, the scale bar is 100 μm in length with analysis locations shown by red circles

anomalies are more variable in the volcanic zircons, e.g., pumice 606A, than zircon in the plutonic clasts. Whole-rock compositions, by contrast, do not show Ce anomalies (Fig. 4k).

Other zircon trace element concentrations also vary significantly, e.g., Hf (~ 5000–25000 ppm) and U (40–5250 ppm, Fig. 6i). In addition, U/Yb varies (0.1–0.5) although generally within a typical igneous zircon range of 0.2–4 (Hoskin and Schaltegger 2003); some values are low in scoria 861, pumice 863A and plutonic clast 862AZ, which is variably attributable to low U and high Yb. The Th/U ratios (0.5–3.6, with only two low values in plutonic clast 616B) are also typical of igneous values ≥ 0.5.

In the Grimes et al. (2015) tectonomagmatic discrimination diagram (Fig. 6j), the mingled deposit zircon compositions straddle the high U/Yb to low U/Yb boundary, falling in the Hawai'i and Iceland 'crustal input or enriched mantle source' fields.

Hf and O isotopes The Mingled Fall zircon Hf isotope data are heterogeneous (Fig. 7A). Zircon Hf isotope ratios are sensitive to magma composition variations, which may reflect source compositions. Depleted mantle has high εHf > 15, whereas enriched sources, e.g., continental crust, have lower values, < 0 (Hawkesworth et al. 2010). Hf isotopes were analysed for zircon from five representative samples: scoria 861 (2.75–13.77); pumices 606A (5.99–9.31) and 863A (5.15–10.11) and plutonic blocks 862A7 (3.15–9.67), 862AZ (6.46–11.45) and 616B (7.63–10.42, and two negative values at ~ − 2 and − 7). The εHf values do not correlate with $\delta^{18}O$, differentiation (Zr/Hf), age nor Ti content.

Mingled Fall zircon O isotope data are also heterogeneous (Fig. 7B). The $\delta^{18}O$ is reported relative to VSMOW; values range from well below typical mantle compositions (4.7–5.9‰) to higher (> 6‰) typical of continental crust (cf. Valley 2003). Oxygen isotopes were analysed for zircon from five representative samples: scorias 863B (4.30–5.78) and 861 (3.49–6.23); pumice 863A (1.58–5.29) and plutonic blocks 862A7 (4.12–5.87) and 862AZ (4.39–6.54). The $\delta^{18}O$ values do not correlate with differentiation (Zr/Hf) nor age.

Geochronology: U–Th–Pb crystallisation ages

Results of the SHRIMP U-Th-Pb analysis and age calculations are shown in Figs. 8 and 9, and the data are presented in Supplementary Material Table 3. Unaltered primary magmatic zircon grains, representative of those separated from each sample, were targeted for dating by avoiding regions apparently affected by hydrothermal alteration with murky or fluid inclusion-rich pitted textures (cf., Hoskin 2005; Jiang et al. 2019). Results from altered grains were eliminated from the dataset when detected, e.g., flat chondrite-normalised LREE patterns and small Ce anomalies from fluid inclusions or tiny inclusions of LREE-rich minerals such as allanite and chevkinite (Hoskin and Schaltegger 2003; Claiborne et al. 2010; Zhong et al. 2021; Ni et al. 2020).

All analyses have variable common lead, originating from the limited radiogenic Pb produced during the short lifespan of the zircon grains. Typically, data points align along common-Pb discordias, where the lower intercepts are interpreted as the age of the sample. Wetherill concordia diagrams were generated for all samples and frequency distributions with relative probability curves were plotted for all 207-corrected $^{206}Pb/^{238}U$ ages permitting visualisation of different zircon populations (Figs. 8 and 9). This combined approach enables identification of age maxima and constraint of crystallisation timing using the lower intercept ages obtained from common Pb discordias in the Wetherill diagram.

Before presenting the geochronological results for each sample in detail, we first discuss the zircon dates in general terms and explain the rationale behind their division into distinct age populations. Firstly, it is important to note that the zircon dates of both the Ascension volcanic deposits, scoria and pumice, are multimodal whereas the plutonic blocks each have one dominant age population, although the probability density function does show other minor peaks (Fig. 9). The decision about which age populations to define and how to group the analyses was based on the distribution of the $^{206}Pb/^{238}U$ ages in Wetherill concordia diagrams. Following standard procedure, analyses that define a discordia line are considered to represent a single age population, whereas older points that do not fit the discordia line and plot above the main age trend are interpreted as inherited grains. The division of the scoria ages into 3 groups, < 0.7 Ma, 0.70–1.0 Ma and > 1.0 Ma, is consistent with and supported by the ages of inherited grains in the pumice samples and, importantly, by the unimodal age ranges of the older plutonic lithic clasts, which provide a robust constraint. In all samples, the data points are, without exception, discordant, an expected feature in zircon grains as young as those analysed, yielding more or less well-defined common lead discordia arrays. The fit of the data points along the discordia lines is never perfect which contributes to the high MSWD values. However, the errors are usually small, and the lower intersection ages for each sample consistently match the weighted mean 207-corrected $^{206}Pb/^{238}U$ ages and, in some cases, show even greater precision.

***Scoria* 863B (Middleton Ridge)** Eighteen zircon grains were selected for U-Th-Pb analysis from scoria 863B (Fig. 8a–c), they are divided into three groups of six grains that align on Wetherill diagram discordia with a lower

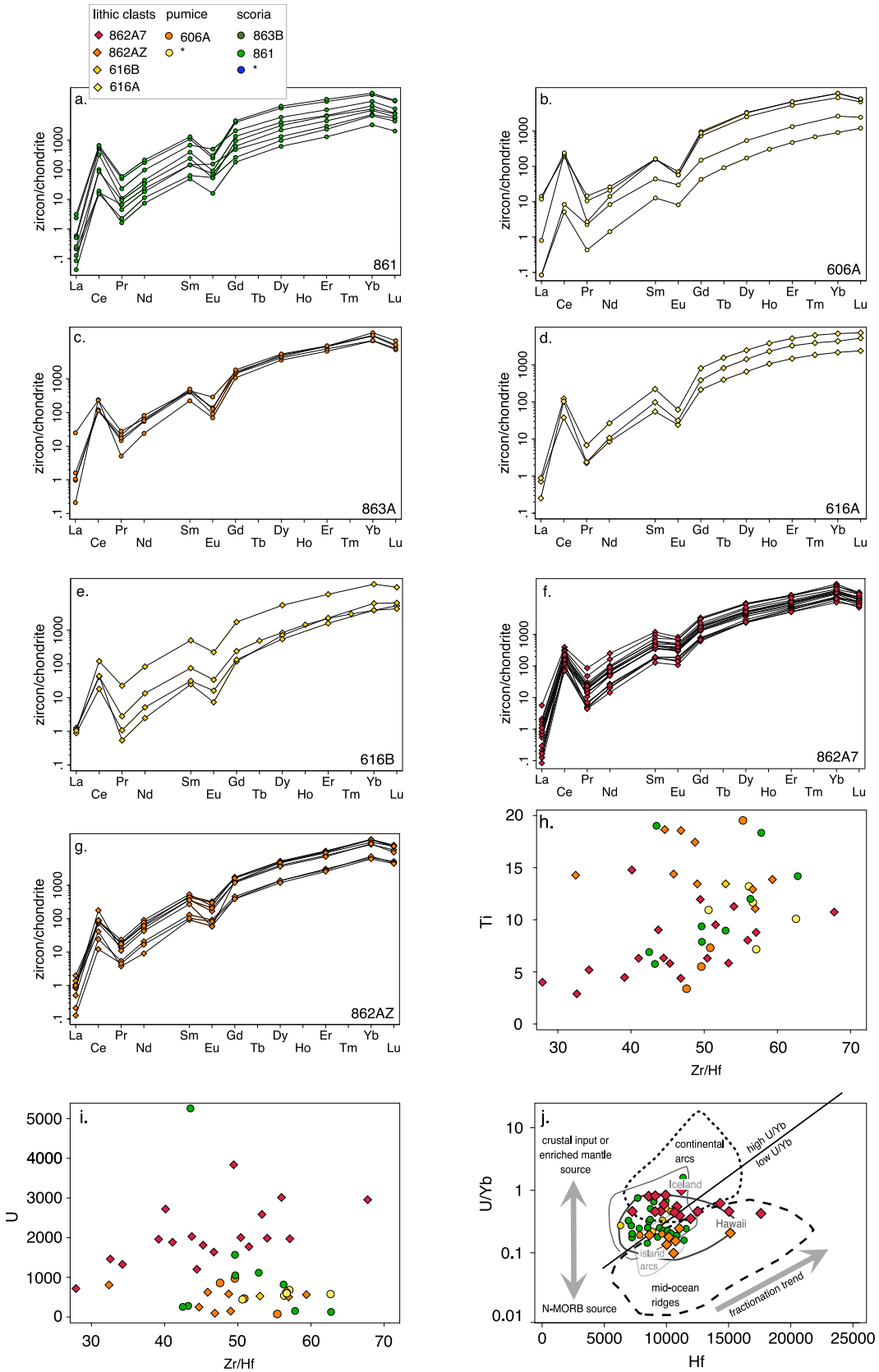
lithic clasts
862A7
862AZ
616B
616A
pumice
606A
*
scoria
863B
861
*
a.
861
b.
606A
c.
863A
d.
616A
e.
616B
f.
862A7
g.
862AZ
zircon/chondrite
La Ce Pr Nd Sm Eu Gd Tb Dy Ho Er Tm Yb Lu
h.
Ti
Zr/Hf
i.
U
Zr/Hf
j.
U/Yb
Hf
crustal input or enriched mantle source
continental arcs
high U/Yb
low U/Yb
Iceland
Hawaii
island arcs
mid-ocean ridges
N-MORB source
fractionation trend

◂**Fig. 6** **a**–**g** Zircon REE normalised to chondrite, normalisation values from McDonough and Sun (1995); **h** Ti vs Zr/Hf; **i** U vs Zr/Hf; **j** zircon U/Yb vs Hf tectonomagmatic discrimination diagram of Grimes et al. (2015), samples plot in the enriched mantle source region of the overlapping Iceland and Hawai'i fields; plutonic clasts 862A7 and 862AZ plot along a parental melt fractionation trend from the volcanic rocks. Trace elements expressed in ppm. *Samples of the same rock types that extend the compositional range are also included in Fig. 4 (cf. Chamberlain et al. 2020 and references therein)

intercept of $0.63+0.12-0.11$ Ma (MSWD 7.56); six more grains have a lower intercept of 0.95 ± 0.15 Ma (MSWD 2.04); and the final six grains have a lower intercept of $1.41+0.33-0.38$ Ma (MSWD = 4.2).

861 (Debris Avalanche) Nineteen zircon grains were selected for U-Th-Pb analysis from scoria 861 (Fig. 8d, e). The 19 analyses are discordant and indicate that there is more than one population: a younger one, nine points, with a lower intersection age 0.64 ± 0.05 Ma (MSWD = 2.17; and an older one, part of which defines, broadly speaking, another discordia, 5 points, lower intercept age 1.24 ± 0.21 (MSWD = 11.8). Four older dispersed ages, 1.3 to 1.8 Ma, were not considered in the Wetherill plots, to avoid overstating the interpretation of distinct age populations.

***Pumice* 606A (Debris Avalanche)** Fourteen zircon grains were selected for U-Th-Pb analysis from pumice 606A (Fig. 8f). The 14 analyses are discordant but define a single population without inheritance that has a lower intercept age $0.60+0.11-0.17$ (MSWD = 0.92). Given the absence of inherited zircon grains, this age is considered to reflect crystallisation of the 'Mingled Fall' eruption.

863A (Middleton Ridge) Nineteen zircon grains were selected for U-Th-Pb analysis from pumice 863A (Fig. 8g, h). The 19 analyses are discordant and indicate that there is more than one population: a younger one of 7 points with a lower intercept age of $0.60+0.10-0.11$ (MSWD = 5.7) and an inherited one of 12 points with a lower intercept age of 1.36 ± 0.2 Ma (MSWD = 18.7).

From these results, summarised in Figs. 8 and 9, it appears reasonable to group all the geochronological data for zircon in the volcanic rocks. Doing this gives an age of 0.60–0.64 Ma**,** which we consider to be the overall crystallisation age of the 'Mingled Fall' eruption.

***Plutonic accidental lithic clasts* 616A (Middleton Ridge)** Nineteen zircon grains were selected for U-Th-Pb analysis from plutonic clast 616A (Fig. 8i). The 19 analyses are discordant but define a single population without evidence of inheritance with a lower intercept age of 0.61 ± 0.05 Ma (MSWD = 8.1).

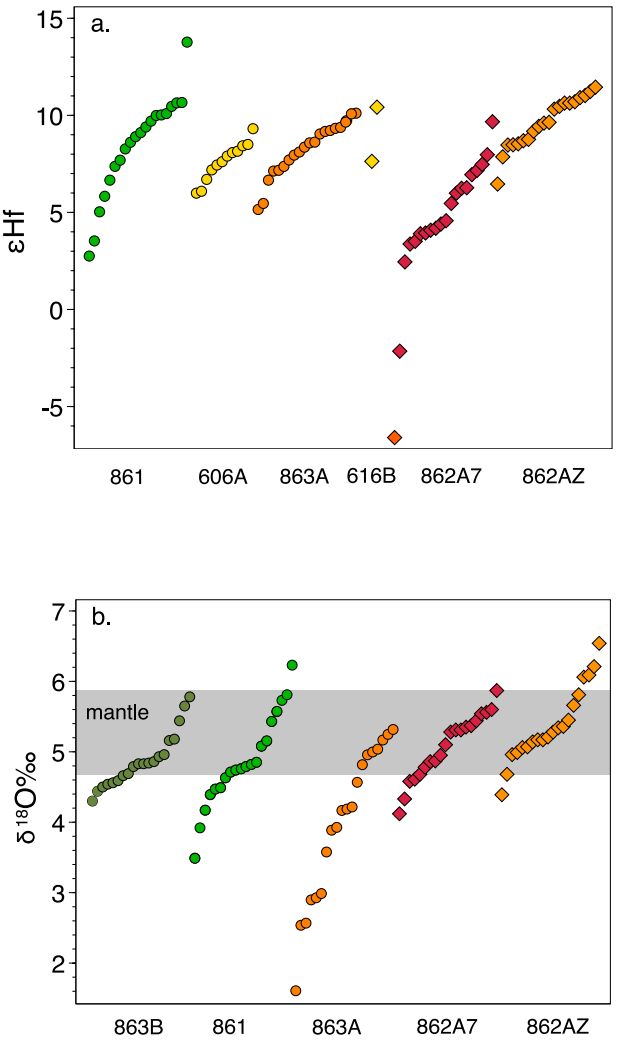

Fig. 7 Zircon isotope compositions. **a** εHf; **b** $\delta^{18}O$ (mantle values marked as a grey band from Valley 2003)

616B (Middleton Ridge) Only six grains were separated from plutonic clast 616B (Fig. 5F) of which four were large enough for U-Th-Pb analysis (Fig. 8j). The four analyses are discordant but define a single population without inheritance and a lower intersection age of $1.28+0.40-0.46$ Ma (MSWD = 8.3).

862A7 (Debris Avalanche) Seventeen zircon grains were selected for U-Th-Pb analysis from plutonic clast 862A7 (Fig. 8k). The 17 analyses are discordant but define a single population without inheritance and a lower intercept age of 0.61 ± 0.03 Ma (MSWD = 2.5).

862AZ (Debris Avalanche) Seventeen zircon grains were selected for U-Th-Pb analysis from the plutonic clast 862AZ (Fig. 8l). The 17 analyses are discordant but define a single

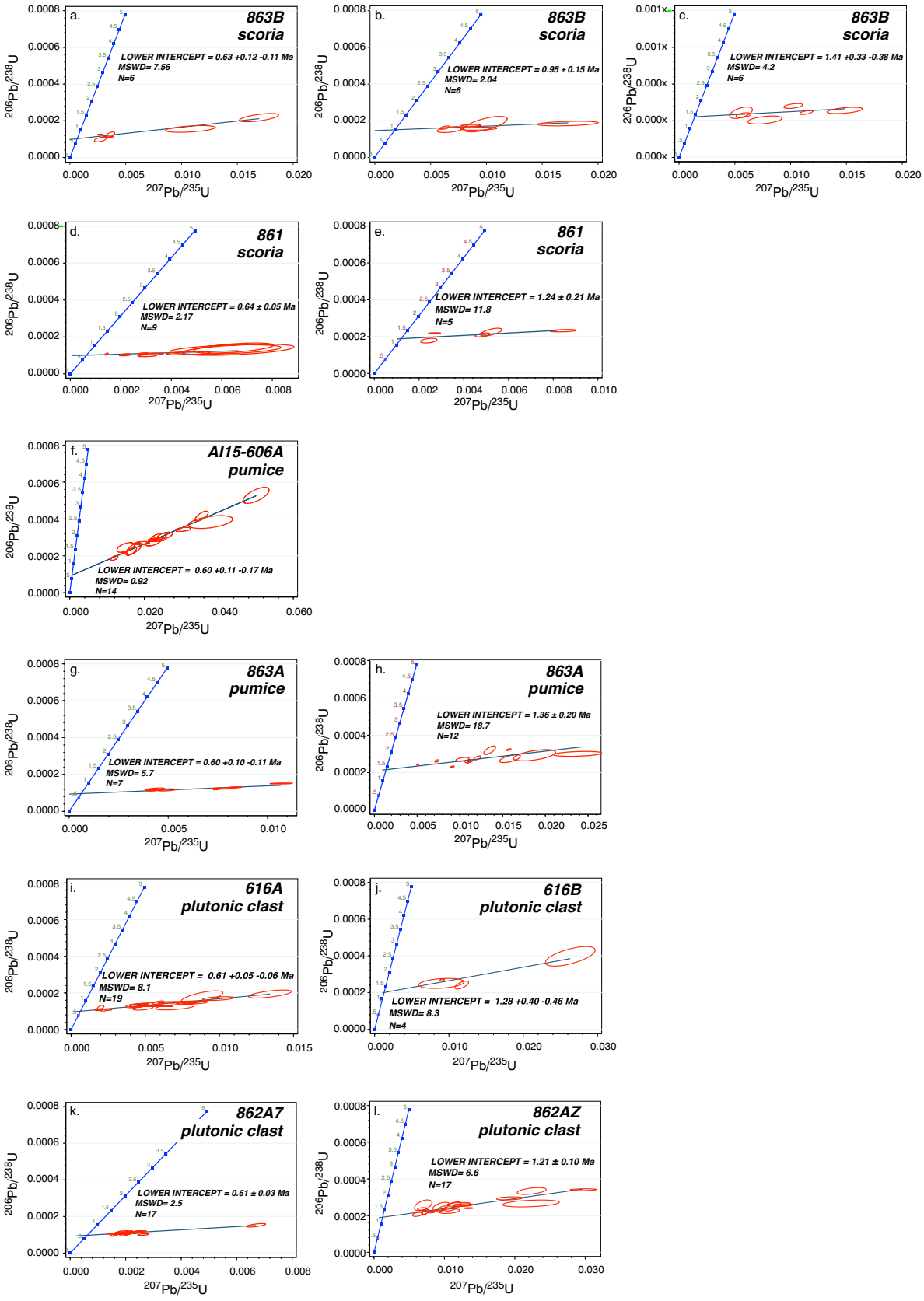

Fig. 8 Wetherill discordia, uncorrected for common Pb

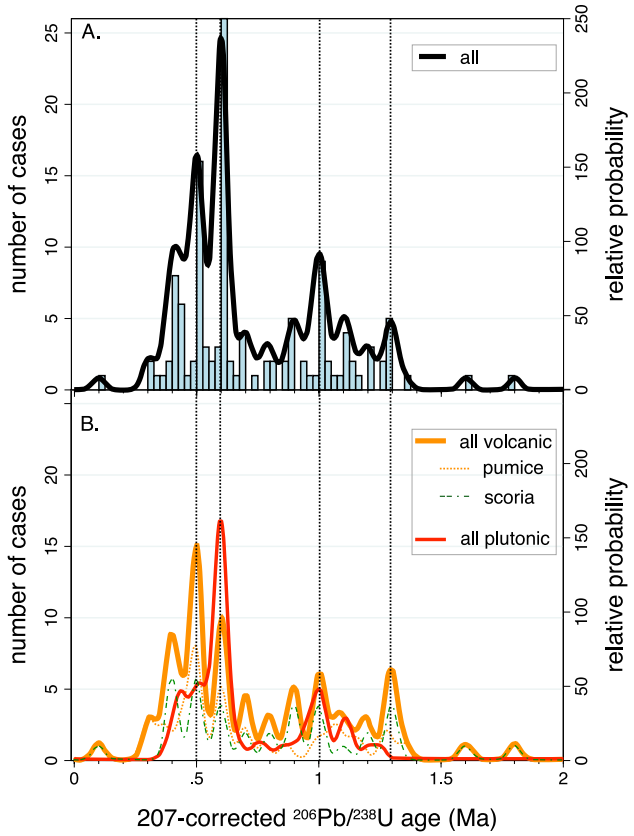

Fig. 9 **a** Histograms and kernel-density curves of the zircon U-Th-Pb ages, all grain analyses. **b** Kernel-density curves of the zircon U-Th-Pb ages of grains from the volcanic and plutonic rocks

population without inheritance and a lower intersection age of 1.21 ± 0.10 Ma (MSWD = 6.6).

Zircon intensive variables

Zircon saturation temperatures

Magma temperature and composition, specifically the Zr content and the *M* value (cation ratio (Na + K + 2Ca)/(Al × Si)), control zircon crystallisation. Using the equations of Boehnke et al. (2013) and whole-rock XRF data, the Mingled Fall zircon saturation temperatures (ZST) were calculated as follows: scorias 710 °C; pumices from this study 740 °C and hotter 860–890 °C for the more evolved pumices of Chamberlain et al. (2020); and accidental lithic clasts older quartz syenite plutonic clasts, 800–840 °C, and younger monzonite, 740 °C, and granite, 955 °C. It should be remembered, however, that whole-rock Zr/Hf suggests neither the accidental lithic plutonic clasts—which show evidence of zircon fractionation—nor the juvenile volcanic deposits—which are mingled—represent single magma batches.

Ti-in-zircon temperatures

The similarity in the composition and ages of the volcanic zircons leads us to combine the data and consider them as one group.

The Ti-in-zircon temperatures (Watson and Harrison 1983; Ferry and Watson 2007) were calculated for all samples with trace element data (scoria 861; pumice 606A and 863A; and plutonic accidental lithic clasts, 862A7, 862AZ, 616A and 616B). Zircon grains with excessively high Ti, > 20 ppm, were eliminated from consideration because these values were attributed to microscopic inclusions of Ti–rich minerals such as Fe-Ti oxides and titanite (cf., Fu et al. 2008). Silica activity $a(SiO_2)$ of 1.0 was used for the volcanic and plutonic accidental lithic clasts calculations because the granitoids, syenites and pumice all contain quartz. Rutile is not present in the Ascension rocks, and titanomagnetite is more abundant than ilmenite (e.g., Harris 1986; Chamberlain et al. 2016, 2019). So, a moderate $a(TiO_2)$ may be inferred because ilmenite crystallises in place of magnetite if Ti is readily available in an Fe-rich system (Buddington and Lindsley 1964). Using the only available magnetite-ilmenite pairs from Mingled Fall scoria (Chamberlain et al. 2020), the equations of Ghiorso and Evans (2008) gave a $a(TiO_2) = \sim 0.5$ (range 0.48–0.59). Similarly, Chamberlain et al. (2016) calculated a $a(TiO_2) = 0.37$ (range 0.32–0.4) for a zoned pumice fall from the Eastern Felsic Complex (Fig. 1). Using the Chamberlain et al. (2020) values, average Ti-in-zircon temperatures were calculated for the zircon in the volcanic deposits: 788 °C (range 650–880 °C), notably the highest temperatures are comparable to the ZST of the most evolved pumices, 860–890 °C. Note that Fe-Ti oxide thermometry and feldspar-melt thermometry for these and similar rocks from nearby outcrops (Chamberlain et al. 2019, 2020) gave value of 900 °C for the scoria but 800 °C for the pumice. For the plutonic accidental lithic clasts, a $a(TiO_2) = 0.55$ was calculated using granite ilmenite-magnetite pairs from Harris (1982), which gave an average Ti-in-zircon temperature of 786 °C (range 690–875 °C). These temperatures were calculated according to Ferry and Watson (2007), with pressure dependence according to Ferriss et al. (2008). They are comparable with estimates for the formation of granitic plutonic bodies at temperatures of 710–865 °C (and pressures of 200–300 MPa, Webster & Rebbert 2001, and references therein; Chamberlain et al. 2020). Independent of the exact numbers, it is clear that the Ti content of the zircon grains varies, and this is, most likely, a result of temperature variation at the time of crystallisation. Although it should be borne in mind that $aTiO_2$ is a dynamic parameter also influenced by melt Ti content and mineral assemblage (Fonseca Teixeira et al. 2023). The calculated temperature would vary by ~ 40° for every 0.1 variation in $aTiO_2$.

Oxygen fugacity

The clear positive anomaly in Ce in the zircon chondrite-normalised diagrams reflects oxidising magmatic conditions as Ce^{+4} is preferentially incorporated into the zircon crystal structure relative to $LREE^{+3}$ and $MREE^{+3}$. Magma oxygen fugacities during crystallisation were calculated from zircon Ti, U and Ce concentrations using the calibration of Loucks et al. (2020); conditions were relatively oxidising, with reference to the ΔFMQ buffer: scoria is in the range + 1.75 to + 4.02; pumices + 0.67 to + 5.07; with little difference between the younger, + 1.56 to + 3.35, and older, + 0.56 to + 2.02, plutonic accidental lithic clasts. These last values are comparable to magma oxygen fugacities calculated from zircon in ~ 0.9 Ma pumice from an explosive-effusive sequence in the Eastern Felsic Complex, + 1.38 to + 3.77 (Scarrow et al. 2023).

Discussion

Here, we combine the geochronological and compositional results to consider the petrogenetic processes that resulted in the Mingled Fall deposit, in particular, the duration of the magmatic system, petrogenetic source processes that generated the juvenile magma scoria and pumice volcanic rocks and associated accidental lithic plutonic clasts, and magma mingling and mineral recycling between different reservoirs and magmatic events.

Zircon geochronological constraints on magma crystallisation timing and plutonic-volcanic links

As noted above, the zircon ages of both the volcanic deposits and the plutonic lithic clasts are broadly bimodal, ca. 0.6 Ma and ca. 1.2–1.4 Ma, indicating prolonged cyclicity in magmatic activity, in summary: scorias 0.63 Ma, 0.67 Ma, 0.95 Ma, 1.34 Ma and 1.4 Ma; pumices 0.60 Ma and 1.36 Ma; and plutonic accidental lithic clasts 0.61 Ma, 1.21 Ma and 1.28 Ma (Fig. 8). The validity of the new 0.6 Ma eruption age for the Mingled Fall is reinforced by Ar/Ar feldspar dating of pumices directly in contact with it, both beneath, 0.693 ± 0.047 Ma, and above, 0.591 ± 0.017 Ma (Preece et al. 2021).

We interpret the older dates to be zircon grains inherited from previous magmatic episodes. These ages are consistent with the timing of several episodes of older volcanic activity dated in the vicinity of the Mingled Fall outcrops (Fig. 1) including the following: volcanic lava clasts in the nearby Echo Canyon explosive pumice deposits, zircon U-Th-Pb 1.34 ± 0.13 Ma (Scarrow et al. 2023); Green Mountain Road pumice, feldspar Ar/Ar, 0.918 ± 0.025 Ma (Preece et al. 2021); and Middleton Ridge rhyolite, Ar/Ar sanidine, 1.094 ± 0.012 Ma, trachyte 0.943 ± 0.007 Ma, as well as dykes 0.931 ± 0.014 Ma and, Ar/Ar groundmass, 0.903 ± 0.006 Ma (Jicha et al. 2013).

Hence, whereas the new Mingled Fall pumice zircon record crystallisation ages of magma erupted at the surface, the plutonic accidental lithic clast ages reveal the timing and distribution of magmatism at depth. This is of relevance for construction of the island because crustal structure, in particular plutonic rocks, apparently exerted a significant control on fractional crystallisation of magma stored in small-volume reservoirs and therefore on the compositional range and eruptive style of volcanic deposits (Chamberlain et al. 2019). Based on stratigraphic mapping and Ar/Ar dated deposits, Preece et al. (2021) recognised two time periods of felsic volcanism, ~ 1 Ma to 0.5 Ma and ~ 0.10–0.05 Ma, with older volcanism predominantly found in the Central Felsic Complex and younger volcanic activity largely confined to the Eastern Felsic Complex (Fig. 1). However, there is less evidence for magmatic separation at depth. Distribution of the early magmatism such as the new > 1 Ma ages for accidental lithic clasts at Echo Canyon (Fig. 1, Scarrow et al. 2023) indicates a plutonic core conditioned magma ascent and differentiation in the east of the island throughout its history, as proposed by Chamberlain et al. (2019).

Furthermore, our new geochronological results shed light on the conundrum of whether plutons preserve magma equivalent to that erupted during volcanic events but solidified at depth (e.g., Metcalf 2004; Miller et al. 2011; Keller et al. 2015; Lipman and Bachmann 2015; Scarrow et al. 2022) or are remnants of the magma source tapped during the volcanic activity (e.g., Bachmann and Bergantz 2004; Eichelberger et al. 2006; Gelman et al. 2014; Glazner et al. 2015; Lundstrom and Glazner 2016; Cashman et al. 2017). Here, the answer appears to be both, even during the same eruption. Only one of the young plutonic clasts, 616A, lies on the extension of the volcanic rock whole-rock major and trace element fractionation trends (Fig. 3), interpreted to record 'unerupted volcanic magma'. The other plutonic clasts, both those that are coeval with the volcanic activity, ~ 0.6 Ma and the older ones ~ 1.3 Ma, are compositionally displaced consistent with mineral accumulation, for example higher Al_2O_3, K_2O and Na_2O as well as Sr values suggesting additional alkali feldspar, preserving remnant source rocks.

Zircon compositional indications of magma source, oxidation conditions, relative crystallisation timing and tectonomagmatic context

The Mingled Fall zircon Hf isotope compositions are heterogeneous, ranging up to > 10 εHf units in a single sample (Fig. 7A), varying from enriched low values (εHf, < 3) to

near depleted mantle compositions (εHf, > 15) (Pettingill and Patchett 1981; Hawkesworth et al. 2010). As with age and trace element results, scoria 861 has the greatest variation in εHf of the volcanic samples, albeit still within the full range of the plutonic accidental lithic clast zircon values. The lack of correlation between εHf and $\delta^{18}O$, differentiation (Zr/Hf), age and Ti content suggests εHf is a primary magmatic characteristic reflecting magma source variation. Parallel chondrite-normalised trace element concentrations (Fig. 6a–g) are indicative of crystallisation from a single magma that had a uniform trace element composition but at the same time presumably preserved isotopic heterogeneities. Comparable broad ranges of εHf were noted in modern island arc rocks by Dhuime et al. (2011) with similar diversity detected in alkaline rocks attributed to recycling of subducted oceanic or continental crustal material into source reservoirs (Zhu et al. 2017).

The Mingled Fall zircon chondite-normalised positive Ce/Ce* anomalies (Fig. 6a–g) are parallel-subparallel, with similar magnitude and shape across multiple zircon grains, recording primary oxidising magmatic conditions (cf., Kelley and Cottrell 2009): displaced relative to the ΔFMQ buffer by + 1.75 to + 4.02 for the scoria and + 0.67 to + 5.07 for the pumices. On the other hand, for all samples except scoria 861, which also has the most varied age profile (Fig. 8), the zircon Eu/Eu* anomalies are negative, and parallel, interpreted to be an artefact of early plagioclase fractionation under more reducing conditions before zircon crystallised (cf., Trail et al. 2012). So, the oxygen fugacity of the magma apparently changed as the magmatic system evolved potentially placing constraints on the relative timing of zircon in the alkaline magmatic system as late stage (cf., Linnen and Keppler 2002; Schmitt et al. 2023), after implied meteoric water or seawater involvement. Specifically, the heterogenous low zircon $\delta^{18}O$ values (Fig. 7B), < 4.7‰, indicate incorporation of high-T, > 300 °C, marine or meteoric water, most likely by assimilation of hydrothermally altered oceanic crust—perhaps driven by latent heat of crystallisation of major mineral phases—prior to crystallisation of at least some of the accessory zircon grains (cf., Adams 1996; Bindeman and Valley 2001; Carley et al. 2014; Jo et al. 2016; Scarrow et al. 2022, 2023).

Tectonomagmatic setting plays a role in determining certain zircon trace element concentrations (Grimes et al. 2015). The intraplate oceanic setting of Ascension Island, 50 km south of the Ascension Fracture Zone and ~ 100 km west of the Mid-Atlantic Ridge, has been linked to both anomalously enriched MORB (Paulick et al. 2010) and a low flux, shallow plume (Gaherty and Dunn 2007). Zircon U/Yb and Hf compositions plot in the Grimes et al. (2015) 'crustal input or enriched mantle source' Iceland and Hawai'i hotspot fields. Some zircon grains principally from the plutonic clast, 862A7, extend to more evolved, higher Hf, compositions along a magmatic fractionation trend from the main dataset (Fig. 6j). Crustal input is ruled out, however, by the mantle or lower $\delta^{18}O$ values, whereas the enriched source component interpretation is supported by Nb/Yb values that are generally greater than 0.01 (Grimes et al 2015).

Zircon compositional and geochronological evidence for magma mingling

Several lines of evidence lead us to conclude that zircon in the scoria was inherited from the pumice magma. First, this is consistent with the whole-rock and major mineral phase compositions, which indicate open system processes, such as a continuum between scoria and pumice compositions (Fig. 4) and complex macrocyst cargoes and disequilibrium textures observed in feldspar, clinopyroxene, forsteritic olivine, and Fe-Ti oxides (Chamberlain et al. 2020). These features led those authors to propose derivation of the scoria from multiple sources. Parenthetically, indications of crystal populations scavenged from pre-existing magmas and plutonic rock bodies highlight the importance of identifying true, equilibrium, minerals for thermobarometric studies. The preservation of complex mafic and felsic interactions in textures, felsic glass selvedge rims and the lack of overgrowth rims on plagioclase and clinopyroxene grains in disequilibrium with the scoria trachybasaltic whole-rock composition indicates that mechanical mingling was late-stage, i.e., just a few hours before eruption (Chamberlain et al. 2020) which is particularly relevant for hazard and risk assessment related to future eruptions. The evidence of rapid cooling is consistent with inhibition of zircon dissolution and its preservation in the mafic melts (cf., Bea et al. 2007; Bea and Montero 2013).

The second line of evidence that the zircon in the scoria was inherited from the pumice magma is the scoria whole-rock zircon saturation temperatures (ZST) of ~ 700 °C; these are cooler than the 900 °C temperature calculated by Fe-Ti oxide and feldspar-melt thermometry (Chamberlain et al. 2019, 2020), indicating the mafic magma was zircon undersaturated when it crystallised. Pumice whole-rock ZST, on the other hand, are hotter, ~ 880 °C, than the corresponding Ti-in-zircon crystallisation temperatures of 780 to 850 °C, indicating zircon saturation. It is also notable that the scoria Ti-in-zircon temperatures are the same as those for the pumice, not hotter, e.g., ~ 900 °C, as would be expected if the zircon had crystallised from a more mafic magma. A caveat in interpretation of ZSTs is the presence of Zr-poor macrocrysts in volcanic rocks which may lead to an underestimation of melt Zr and so the ZSTs (Harrison et al. 2007). Conversely, an accumulation of ante- or xenocrystic zircon may result in an increase in ZSTs, e.g., a 500-ppm increase in Zr would raise the calculated temperature by ~ 80 °C. Even considering this potential artefact, the scoria ZSTs would still

fall below the crystallisation temperatures, indicating undersaturation. In any case, the predominantly glassy textures of both the Mingled Fall scoria and pumice (5–10 modal% and 5 modal% macrocrysts, respectively) attest to the validity of the calculated volcanic ZSTs.

Thirdly, and apparently paradoxically, as noted above the scoria, zircon grains have more scattered ages. In addition to the plotted geochronological data (Figs. 8 and 9), the scoria also contained grains with older, dispersed ages. Moreover, zircon from the scoria has the most heterogeneous trace element compositions (Fig. 6). This paradox may be explained if the mafic magma incorporated extraneous crystals not only from the rhyolitic end member, but also from other preexisting plutonic and volcanic rocks, because its ascent was more erosive, because it was hotter and more explosive, than the immediately preceding felsic eruption. Comparable heterogeneity is observed in the scoria macrocryst mineral phases (Chamberlain et al. 2020). Notably, the scoria is more vesicular, 40–50 modal%, than the pumices, 30–40 modal%. Accordingly, although centimetric-scale plutonic clasts are present in pumice and scoria from both outcrops, they are appreciably more abundant in the latter. As during the ~ 0.95 Ma Echo Canyon felsic explosive-effusive eruption to the east of the Mingled Fall (Fig. 1, Scarrow et al. 2023), most lithic material was apparently mobilised from the volcanic edifice and sub-volcanic plutonic system via increased energy during the eruptive paroxysm.

Finally, zircon trace element concentrations also record evidence of mingling (e.g., Figure 6h, i). Similarities exist between trends in the age data and Zr/Hf differentiation index ranges in the volcanic rock zircon grains. Pumice 606A has one single 0.6 Ma zircon age population and the most restricted Zr/Hf range, apparently crystallised from the same rhyolitic magma. On the other hand, the scoria 861 zircon, that records variable age populations, 0.6 Ma and 1.2 Ma, also has the broadest volcanic range in Zr/Hf. Only the 0.6 Ma monzonite accidental lithic clast, 862A7, has a more extensive range of zircon Zr/Hf values than the scoria, which is consistent with the plutonic accidental lithic clast recording syn-volcanic preservation of compositionally diverse magma at depth. A similar, albeit somewhat more limited, variation in zircon Zr/Hf is also preserved in the quartz syenite 862AZ. Thus, we suggest that the restricted zircon compositional range in 606A records the zircon crystallised from the contemporaneous gabbro-melt rhyolite magma, whereas the broader range in other volcanic rocks reflects exotic grains scavenged from the plutonic or past active melt systems and, perhaps other as yet unidentified, components. Some compositional characteristics, for example higher U in plutonic clast 862A7 than any other sample (Fig. 6i), suggest it may be possible to unravel the source to sink path of individual grains. Although beyond the scope of the current study, this possibility merits further investigation.

Petrogenetic model for the Mingled Fall magmatic processes

Field observations are combined with whole-rock geochemical and petrographic compositions, major phase mineral data (Chamberlain et al. 2020) and new zircon ages, isotope and trace element chemistry to decipher timing of magma storage, source character and magma mingling. The main stages of the petrogenetic model are summarised below; numbers refer to Fig. 10.

1. The generation of significant melt to create plutons, ca. 1.3–1.2 Ma, recorded in accidental lithic clasts erupted at the Mingled Fall outcrops, confirms widespread felsic magmatism during the early history of central Ascension Island. There are no (remaining) volcanic deposits of this age, but coeval felsic volcanism is found elsewhere on the island (Jicha et al. 2013; Preece et al. 2021).
2. Mantle melting led to crystallisation of mafic magma as lower crustal gabbro; this subsequently melted to produce evolved rhyolitic melts, inferred to have formed shortly before crystallisation, at ca. 0.6 Ma. This process also involved the assimilation of high-T hydrothermally altered country rock prior to accessory mineral crystallisation, as recorded in zircon O isotopes.
3. Zircon crystallisation from felsic magmas at 0.60 Ma is recorded in both the accidental plutonic lithic clasts formed at depth and the erupted juvenile volcanic pumice. Trace element compositions indicate an enriched mantle source, and although no clear continental crustal component was detected in the zircon O isotopes, the zircon Hf isotopes are intermediate between depleted mantle and enriched source values.
4. Intrusion of volatile-rich mafic, mantle-derived, magma into the felsic melt which resulted in mingling—indicated by field characteristics, major mineral phase disequilibrium (Chamberlain et al. 2020) and recorded in the scoria by zircon with comparable age and composition to the rhyolite, pumice, magma. This mingling triggered the explosive eruptive process.
5. Compositional stratification resulted from the early stage of the eruption tapping more evolved magmas, producing pumice, then the later stage of the eruption, scoria, with mineralogical evidence of mingling between the two.

Questions remain regarding the conditions that led to the eruption of both mafic and felsic melts in the specific instance of the Mingled Fall. Does this reflect a stochastic

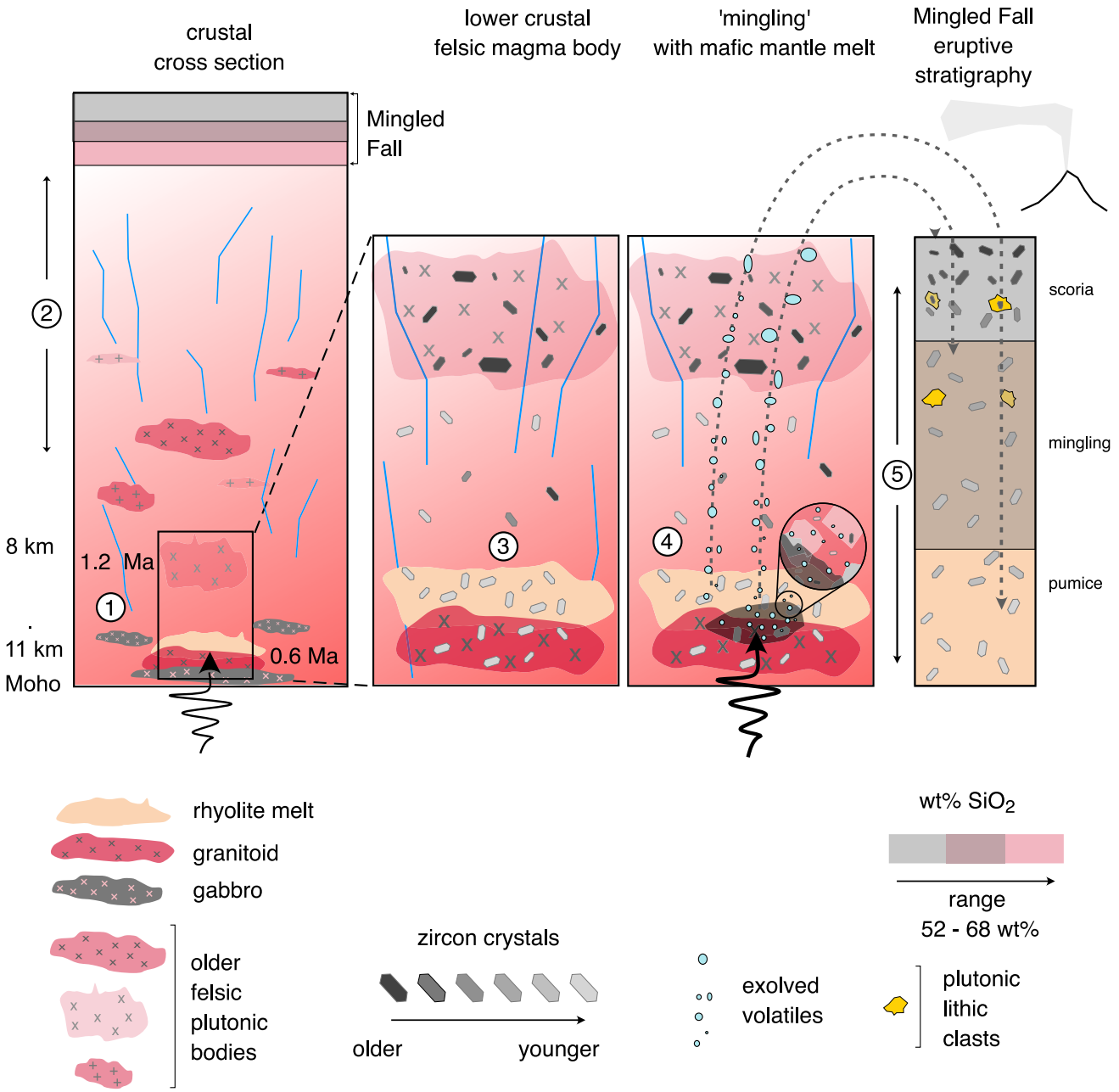

Fig. 10 Schematic representation of the chronology and processes in the Mingled Fall magmatic system. Key aspects are labelled with numbers relating to the text section 'Petrogenetic model for the Mingled Fall magmatic processes'. The crustal cross-section highlights mantle input, the depth of melt evolution and the proposed position of previous eruptive products relative to the Debris Avalanche and Middleton Ridge stratigraphic sequence. Hydrothermal alteration pathways are represented by irregular vertical blue lines. The magma system shows a variation in wt% SiO_2 and zircon age ranges. The zoom lens shows the interaction between the felsic and mafic magma and highlights the exsolution volatiles. Zircon colour ages are schematic. The erupted Mingled Fall stratigraphy summarises the explosive evacuation of the mingled magma reservoir, first dominantly pumice then scoria. Not to vertical scale

process, where only a small proportion of mafic pulses randomly encounter an active felsic melt pocket, triggering an eruption? Alternatively, could other, more systematic processes—related to either rhyolite generation, basalt ascent, or both—be involved? Looking ahead to future work, targeted research on this topic could result in deeper understanding of the hazards associated with volcanism on remote ocean islands.

Conclusions and implications

Analysis of zircon ages and compositions from the pumice and scoria of a mingled fall on Ascension Island has provided valuable insights into magmatic history and processes that could not be obtained from whole-rock compositions or major mineral phase chemistry alone. Zircon U-Th-Pb ages reveal prolonged, cyclical, magmatic activity with bimodal crystallisation ages, at ~ 1.3 Ma and ~ 0.6 Ma. These results underscore the largely untapped potential of U-Th-Pb SHRIMP dating to determine the ages of zircon in recent Quaternary volcanic rocks.

The zircon isotopic and trace element compositions reveal the enriched character of magmatic source and variable redox conditions during crystallisation. Our O isotope data suggest that assimilation of hydrothermally altered oceanic crust by mantle-derived magmas with heterogeneous Hf isotope values occurred prior to zircon crystallisation. Additionally, varying zircon Ce and Eu anomalies indicate a transition in the magma oxidation state from reducing to more oxidising over time.

Geochronological and compositional constraints combined with intensive variables are consistent with explosive eruption of lower crustal gabbro-melt rhyolitic magma being triggered by mingling with mafic mantle-derived magma. This interaction is recorded in zircon grains preserved in the Mingled Fall pumice and scoria.

In addition, the eruption of the Mingled Fall was at 0.6 Ma and older magmatism points to a cyclicity of 0.6 Ma, so caution is warranted. Given recent Ar/Ar basalt groundmass dating (Preece et al. 2018) has identified the island's magmatic system as active, ~ 500 years old; ongoing detailed studies of the volcanism are particularly pertinent.

Deciphering crystal provenance and residence times not only constrains past magmatic timescales, duration and cyclicity, but also informs potential future activity by enhancing understanding of magma source characteristics, pre-eruptive processes and sub-volcanic melt distribution which is important for efficient volcanic hazard monitoring.

Supplementary Information The online version contains supplementary material available at https://doi.org/10.1007/s00445-025-01848-7.

Acknowledgements We are grateful to Roberto Sulpizio for his editorial handling and to two anonymous reviewers for the time and effort they took to help us improve the clarity and rigour of our data presentation and interpretations—they provided a great combination of positivity from Reviewer 1 and unmatched attention to detail from Reviewer 2. This project received funding from the European Union's Horizon 2020 research and innovation programme under the Marie Skłodowska-Curie grant agreement No. 749611 (JHS). The work was also financially supported by the Spanish grant CGL 2017-84469-P (JHS). KJC acknowledges the Japan Society for the Promotion of Science postdoctoral fellowship #PE16724. Funding for open access charge: Universidad de Granada/CBUA. Richard J. Brown and Bridie V. Davies are thanked for their help with fieldwork. This is IBERSIMS publication Nº: 121.

Author contribution JHS: conceptualization, data curation, formal analysis, funding acquisition, investigation, project administration, visualization, writing—original draft.

KJC: conceptualization, data curation, funding acquisition, investigation, writing—review and editing.

PM: formal analysis, data curation, investigation, methodology, visualization, writing—review and editing.

MSAH: formal analysis, data curation, funding acquisition, methodology.

JB: conceptualization, funding acquisition, investigation, project administration, writing—review and editing.

Funding Funding for open access publishing: Universidad de Granada/CBUA. This project received funding from the European Union's Horizon 2020 research and innovation programme under the Marie Skłodowska-Curie grant agreement No. 749611 (JHS). The work was also financially supported by the Spanish grant CGL 2017–84469-P (JHS and PM) and the Japan Society for the Promotion of Science postdoctoral fellowship #PE16724 (KJC).

Data availability The authors confirm that the data supporting the findings of this study are available within the article and its supplementary materials.

Code availability Not applicable.

Declarations

Conflict of interest The authors declare no competing interests.

References

Adams MC (1996) Chemistry of fluids from Ascension #1, a deep geothermal well on Ascension Island, South Atlantic Ocean. Geothermics 25:561–579. https://doi.org/10.1016/0375-6505(96)00011-9

Ahrens LH, Erlank AJ (1969) Hafnium. In: Wedepohl KH (ed) Handbook of geochemistry 2. B–O. Springer Berlin

Angelo P (2013) Petrogenesis of trachyte and rhyolite magmas on Ponza Island (Italy) and its relationship to the Campanian magmatism. J Volcanol Geotherm Res 267:15–29. https://doi.org/10.1016/j.jvolgeores.2013.09.008

Araña V, Martí J, Aparicio A, García-Cacho L, García-García R (1994) Magma mixing in alkaline magmas: an example from Tenerife. Canary Islands Lithos 32(1–2):1–19. https://doi.org/10.1016/0024-4937(94)90018-3

Bachmann O, Bergantz GW (2004) On the origin of crystal-poor rhyolites: extracted from batholithic crystal mushes. J Petrol 45:1565–1582. https://doi.org/10.1093/petrology/egh019

Bea F, Montero P (2013) Diffusion-induced disturbances of the U-Pb isotope system in pre-magmatic zircon and their influence on

SIMS dating: a numerical study. Chem Geol 349:1–17. https://doi.org/10.1016/j.chemgeo.2013.04.014
Bea F, Montero P, González-Lodeiro F, Talavera C (2007) Zircon inheritance reveals exceptionally fast crustal magma generation processes in Central Iberia during the Cambro-Ordovician. J Petrol 48:2327–2339. https://doi.org/10.1093/petrology/egm061
Bindeman IN, Valley JW (2001) Low-$\delta^{18}O$ rhyolites from Yellowstone: magmatic evolution based on analyses of zircons and individual phenocrysts. J Petrol 42:1491–1517. https://doi.org/10.1093/petrology/42.8.1491
Bindeman IN, Valley JW, Wooden JL, Persing HM (2001) Post-caldera volcanism: in situ measurement of U-Pb age and oxygen isotope ratio in Pleistocene zircons from Yellowstone caldera. Earth Planet Sci Lett 189:197–206. https://doi.org/10.1016/S0012-821X(01)00358-2
Bindeman IN, Gurenko A, Carley T, Miller C, Martin E, Sigmarsson O (2012) Silicic magma petrogenesis in Iceland by remelting of hydrothermally altered crust based on oxygen isotope diversity and disequilibria between zircon and magma with implications for MORB. Terra Nova 24:227–232. https://doi.org/10.1111/j.1365-3121.2012.01058.x
Boehnke P, Watson EB, Trail D, Harrison TM, Schmitt AK (2013) Zircon saturation re-revisited. Chem Geol 351:324–334. https://doi.org/10.1016/j.chemgeo.2013.05.028
Buddington AF, Lindsley DH (1964) Iron-titanium oxide minerals and synthetic equivalents. J Petrol 5(2):310–357. https://doi.org/10.1093/petrology/5.2.310
Carley TL, Miller CF, Wooden JL, Bindeman IN, Barth AP (2011) Zircon from historic eruptions in Iceland: reconstructing storage and evolution of silicic magmas. Miner Pet 102:135–161. https://doi.org/10.1007/s00710-011-0169-3
Carley TL, Miller CF, Wooden JL, Padilla AJ, Schmitt AK, Economos RC, Bindeman IN, Jordan BT (2014) Iceland is not a magmatic analog for the Hadean: evidence from the zircon record. Earth Planet Sci Lett 405:85–97. https://doi.org/10.1016/j.epsl.2014.08.015
Cashman KV, Sparks RSJ, Blundy JD (2017) Vertically extensive and unstable magmatic systems: a unified view of igneous processes. Science 355. https://doi.org/10.1126/science.aag3055
Chamberlain KJ, Barclay J, Preece KJ, Brown RJ, Davidson JP, Edmonds M (2016) Origin and evolution of silicic magmas at ocean islands: perspectives from a zoned fall deposit on Ascension Island, South Atlantic. J Volcanol Geotherm Res 327:349–360. https://doi.org/10.1016/j.jvolgeores.2016.08.014
Chamberlain KJ, Barclay J, Preece KJ, Brown RJ, Davidson JP (2019) Lower crustal heterogeneity and fractional crystallization control evolution of small-volume magma batches at ocean island volcanoes (Ascension Island, South Atlantic). J Petrol 60:1489–1522. https://doi.org/10.1093/petrology/egz037
Chamberlain KJ, Barclay J, Preece KJ, Brown RJ, McIntosh IM, Edmonds M (2020) Deep and disturbed: conditions for formation and eruption of a mingled rhyolite at Ascension Island South Atlantic. Volcanica. 3:139–153. https://doi.org/10.30909/vol.03.01.139153
Cisneros de León A, Schmitt AK (2019) Intrusive reawakening of El Chichón volcano prior to its Holocene eruptive hyperactivity. J Volcanol Geotherm Res 377:53–68. https://doi.org/10.1016/j.jvolgeores.2019.04.004
Claiborne LL, Miller CF, Walker BA, Wooden JL, Mazdab FK, Bea F (2006) Tracking magmatic processes through Zr/Hf ratios in rocks and Hf and Ti zoning in zircons: an example from the Spirit Mountain batholith, Nevada. Miner Mag 70:517–543. https://doi.org/10.1180/0026461067050348
Claiborne LL, Miller CF, Flanagan DM, Clynne MA, Wooden JL (2010) Zircon reveals protracted magma storage and recycling beneath Mount St. Helens Geology 38:1011–1014. https://doi.org/10.1130/G31285.1
Coutts DS, Matthews WA, Hubbard SM (2019) Assessment of widely used methods to derive depositional ages from detrital zircon populations. Geosci Front 10(4):1421–1435. https://doi.org/10.1016/j.gsf.2018.11.002
Daly RA (1925) The geology of Ascension Island. Proc Am Acad Arts Sci 6:3–80
Danišík M, Schmitt AK, Stockli DF, Lovera OM, Dunkl I, Evans NJ (2017) Application of combined U-Th-disequilibrium/U-Pb and (U-Th)/He zircon dating to tephrochronology. Quat Geochronol 40:23–32. https://doi.org/10.1016/j.quageo.2016.07.005
Davies BV (2021) Critical eruptive controls of an intra-plate volcano: Ascension Island South Atlantic. PhD Thesis. Univ East Anglia United Kingdom
Dhuime B, Hawkesworth C, Cawood P (2011) When continents formed. Science 331:154–155. https://doi.org/10.1126/science.1201245
Eichelberger JC, Izbekov PE, Browne BL (2006) Bulk chemical trends at arc volcanoes are not liquid lines of descent. Lithos 87:135–154. https://doi.org/10.1016/j.lithos.2005.05.006
Famin V, Paquez C, Danišík M, Gardiner NJ, Michon L, Kirkland CL, Berthod C, Friedrichs B, Schmitt AK, Monié P (2022) Multitechnique geochronology of intrusive and explosive activity on Piton des Neiges Volcano, Réunion Island. Geochem Geophys Geosys 23. https://doi.org/10.1029/2021GC010214
Ferriss EDA, Essene EJ, Becker U (2008) Computational study of the effect of pressure on the Ti-in-zircon geothermometer. Eur J Mineral 20:745–755. https://doi.org/10.1127/0935-1221/2008/0020-1860
Ferry JM, Watson EB (2007) New thermodynamic models and revised calibrations for the Ti-in-zircon and Zr-in-rutile thermometers. Contrib Mineral Petrol 154:429–437. https://doi.org/10.1007/s00410-007-0201-0
Fonseca Teixeira LM, Troch J, Bachmann O (2023) The dynamic nature of aTiO2: implications for Ti-based thermometers in magmatic systems. Geology 52(1):92–96. https://doi.org/10.1130/G51587.1
Freundt A, Schmincke HU (1992) Mixing of rhyolite, trachyte and basalt magma erupted from a vertically and laterally zoned reservoir, composite flow P1 Gran Canaria. Contrib Mineral Petrol 112:1–19. https://doi.org/10.1007/BF00310952
Friedrichs B, Atıcı G, Danišík M, Atakay E, Çobankaya M, Harvey JC, Yurteri E, Schmitt AK (2020) Late Pleistocene eruptive recurrence in the post-collisional Mt. Hasan stratovolcanic complex (Central Anatolia) revealed by zircon double-dating. J Volcanol Geotherm Res. 404:107007. https://doi.org/10.1016/j.jvolgeores.2020.107007
Friedrichs B, Atıcı G, Danišík M, Yurteri E, Schmitt AK (2021) Sequence modeling in zircon double-dating of early Holocene Mt. Erciyes domes (Central Anatolia). Quat Geochronol. 61. https://doi.org/10.1016/j.quageo.2020.101129
Fu B, Page FZ, Cavosie AJ, Fournelle J, Kita NT, Lackey JS, Wilde SA, Valley JW (2008) Ti-in-zircon thermometry: applications and limitations. Contrib Mineral Petrol 156:197–215. https://doi.org/10.1007/s00410-008-0281-5
Gaherty JB, Dunn RA (2007) Evaluating hot spot–ridge interaction in the Atlantic from regional-scale seismic observations. Geochem Geophys Geosys 8:Q05006. https://doi.org/10.1029/2006GC001533
Gelman SE, Deering CD, Bachmann O, Huber C, Gutierrez FJ (2014) Identifying the crystal graveyards remaining after large silicic eruptions. Earth Planet Sci Lett 403:299–306. https://doi.org/10.1016/j.epsl.2014.07.005
Ghiorso MS, Gualda GA (2015) An H2O–CO2 mixed fluid saturation model compatible with rhyolite-melts. Contrib Mineral Petrol 169. https://doi.org/10.1007/s00410-015-1141-8
Ghiorso MS, Evans BW (2008) Thermodynamics of rhombohedral oxide solid solutions and a revision of the Fe-Ti two-oxide geothermometer and oxygen-barometer. Am J Sci 3:957–1039. https://doi.org/10.2475/09.2008.01

Glazner AF, Coleman DS, Mills RD (2015) The volcanic-plutonic connection. In: Breitkreuz C, Rocchi S (eds) Physical geology of shallow magmatic systems, dykes, sills, and laccoliths. Springer, New York, pp 61–82

González-García D, Boulesteix T, Klügel A et al (2023) Bubble-enhanced basanite–tephrite mixing in the early stages of the Cumbre Vieja 2021 eruption, La Palma. Canary Islands Sci Rep 13:14839. https://doi.org/10.1038/s41598-023-41595-3

Grimes CB, Wooden JL, Cheadle MJ, John BE (2015) "Fingerprinting" tectono-magmatic provenance using trace elements in igneous zircon. Contrib Mineral Petrol 170:46. https://doi.org/10.1007/s00410-015-1199-3

Hanchar JM, Hoskin PWO (2003) Zircon. In: Hanchar JM, Hoskin PWO (eds) Reviews in mineralogy and geochemistry. Mineral Soc Am Chantilly USA. 53

Harris C (1986) A quantitative study of magmatic inclusions in the plutonic ejecta of Ascension Island. J Petrol 27(1):251–276. https://doi.org/10.1093/petrology/27.1.251

Harris C (1982) Coarse-grained rocks of Ascension Island. PhD Thesis. Univ Oxford United Kingdom

Harrison TM, Watson EB, Aikman AB (2007) Temperature spectra of zircon crystallization in plutonic rocks. Geology 35:635–638. https://doi.org/10.1130/G23505A.1

Hawkesworth CJ, Dhuime B, Pietranik AB, Cawood PA, Kemp AIS, Storey CD (2010) The generation and evolution of the continental crust. J Geol Soc 167(2):229–248. https://doi.org/10.1144/0016-76492009-072

Hildreth W (1981) Gradients in silicic magma chambers: implications for lithospheric magmatism. J Geophys Res Solid Earth 86:10153–10192. https://doi.org/10.1029/JB086iB11p10153

Hofmann AW (1988) Chemical differentiation of the Earth: the relationship between mantle continental crust, and oceanic crust. Earth Planet Sci Lett 90:297–314. https://doi.org/10.1016/0012-821X(88)90132-X

Hoskin PWO (2005) Trace-element composition of hydrothermal zircon and the alteration of Hadean zircon from the Jack Hills. Australia Geochim Cosmochim Acta 69(3):637–648. https://doi.org/10.1016/j.gca.2004.07.006

Hoskin PWO, Schaltegger U (2003) The composition of zircon and igneous and metamorphic petrogenesis. In: Hanchar JM Hoskin PWO (eds) Zircon. Rev Mineral Geochem Mineral Soc Am Chantilly USA 53 27–62

Jiang WC, Li H, Evans NJ, Wu JH (2019) Zircon records multiple magmatic-hydrothermal processes at the giant Shizhuyuan W-Sn–Mo–Bi polymetallic deposit. South China Ore Geol Rev 115:103160. https://doi.org/10.1016/j.oregeorev.2019.103160

Jicha BR, Singer BS, Valentine MJ (2013) $^{40}Ar/^{39}Ar$ geochronology of subaerial Ascension Island and a re-evaluation of the temporal progression of basaltic to rhyolitic volcanism. J Petrol 54:2581–2596. https://doi.org/10.1093/petrology/egt058

Jo HJ, Cheong CS, Ryu JS, Kim N, Yi K, Jung H, Li XH (2016) In-situ oxygen isotope records of crustal self-cannibalization selectively captured by zircon crystals from high-δ26Mg granitoids. Geology 44:339–342. https://doi.org/10.1130/G37725.1

Kar A, Weaver B, Davidson J, Colucci M (1998) Origin of differentiated volcanic and plutonic rocks from Ascension Island, South Atlantic Ocean. J Petrol 39:1009–1024. https://doi.org/10.1093/petrology/39.5.1009

Keller CB, Schoene B, Barboni M, Samperton KM, Husson JM (2015) Volcanic–plutonic parity and the differentiation of the continental crust. Nature 523:301–307. https://doi.org/10.1038/nature14584

Kelley KA, Cottrell E (2009) Water and the oxidation state of subduction zone magmas. Science 325:605–607. https://doi.org/10.1126/science.1174156

Kimura K, Hayasaka Y (2019) Zircon U-Pb age and Nd isotope geochemistry of latest Neoproterozoic to early Paleozoic Oeyama ophiolite: evidence for oldest MORB-type oceanic crust in Japanese accretionary system and its tectonic implications. Lithos 342–343:345–360. https://doi.org/10.1016/j.lithos.2019.06.001

Kirkland CL, Danišík M, Marsden R, Piilonen P, Barham M, Sutherland L (2020) Dating young zircon: a case study from Southeast Asian megacrysts. Geochim Cosmochim Acta 274:1–19. https://doi.org/10.1016/j.gca.2020.01.013

Klingelhöfer F, Minshull TA, Blackman DK, Harben P, Childers V (2001) Crustal structure of Ascension Island from wide-angle seismic data: implications for the formation of near-ridge volcanic islands. Earth Planet Sci Lett 190:41–56. https://doi.org/10.1016/S0012-821X(01)00362-4

Laeger K, Petrelli M, Morgavi D et al (2019) Pre-eruptive conditions and triggering mechanism of the ~16 ka Santa Bárbara explosive eruption of Sete Cidades Volcano (São Miguel, Azores). Contrib Mineral Petrol 174:11. https://doi.org/10.1007/s00410-019-1545-y

Linnen RL, Keppler H (2002) Melt composition control of Zr/Hf fractionation in magmatic processes. Geochim Cosmochim Acta 66(18):3293–3301. https://doi.org/10.1016/S0016-7037(02)00924-9

Lipman PW, Bachmann O (2015) Ignimbrites to batholiths: integrating perspectives from geological, geophysical, and geochronological data. Geosphere 11:705–743. https://doi.org/10.1130/GES01091.1

Loucks RR, Fiorentini ML, Henríquez GJ (2020) New magmatic oxybarometer using trace elements in zircon. J Petrol. https://doi.org/10.1093/petrology/egaa034

Lundstrom CC, Glazner AF (2016) Silicic magmatism and the volcanic–plutonic connection. Elements 12:91–96. https://doi.org/10.2113/gselements.12.2.91

Marsden RC, Danišík M, Ahn US, Friedrichs B, Schmitt AK, Kirkland CL, McDonald BJ, Evans NJ (2021a) Zircon double-dating of Quaternary eruptions on Jeju Island. South Korea J Volcanol Geotherm Res 410:107171. https://doi.org/10.1016/j.jvolgeores.2020.107171

Marsden RC, Danišík M, Ito H, Kirkland CL, Evans NJ, Miura D, Friedrichs B, Schmitt AK, Uesawa S, Daggitt ML (2021b) Considerations for double-dating zircon in secular disequilibrium with protracted crystallisation histories. Chem Geol 581:120408. https://doi.org/10.1016/j.chemgeo.2021.120408

Matthews NE, Vazquez JA, Calvert AT (2015) Age of the Lava Creek supereruption and magma chamber assembly at Yellowstone based on $^{40}Ar/^{39}Ar$ and U-Pb dating of sanidine and zircon crystals. Geochem Geophys Geosyst 16:2508–2528. https://doi.org/10.1002/2015GC005881

McDonough WF, Sun SS (1995) The composition of the Earth. Chem Geol 120:223–253. https://doi.org/10.1016/0009-2541(94)00140-4

Metcalf RV (2004) Volcanic-plutonic links, plutons as magma. Trans R Soc Edinburgh Earth Sci 95:357–374. https://doi.org/10.1130/0-8137-2389-2.357

Miller CF, Furbish DJ, Walker BA, Claiborne LL, Koteas GC, Bleick HA, Miller JS (2011) Growth of plutons by incremental emplacement of sheets in crystal-rich host: evidence from Miocene intrusions of the Colorado River region Nevada USA. Tectonophysics 500:65–77. https://doi.org/10.1016/j.tecto.2009.07.011

Minshull TA, Ishizuka O, Garcia-Castellanos D (2010) Long-term growth and subsidence of Ascension Island: constraints on the rheology of young oceanic lithosphere. Geophys Res Lett 37:L23306. https://doi.org/10.1029/2010GL045112

Ni Z, Arevalo R, Piccoli P, Reno BL (2020) A novel approach to identifying mantle-equilibrated zircon by using trace element chemistry. Geochem Geophys Geosyst 21:e2020GC009230. https://doi.org/10.1029/2020GC009230

Paulick H, Münker C, Schuth S (2010) The influence of small-scale mantle heterogeneities on mid-ocean ridge volcanism: evidence from the southern Mid-Atlantic Ridge (7°30′S to 11°30′S) and Ascension Island. Earth Planet Sci Lett 296:299–310. https://doi.org/10.1016/j.epsl.2010.05.009

Pettingill HS, Patchett PJ (1981) Lu-Hf total-rock age for the Amitsoq gneisses, West Greenland. Earth Planet Sci Lett 55:150–156. https://doi.org/10.1016/0012-821X(81)90093-5

Preece K, Mark DF, Barclay J, Cohen BE, Chamberlain KJ, Jowitt C, Vye-Brown C, Brown RJ, Hamilton S (2018) Bridging the gap: $^{40}Ar/^{39}Ar$ dating of volcanic eruptions from the 'Age of Discovery.' Geology 46:1035–1038. https://doi.org/10.1130/g45415.1

Preece K, Barclay J, Brown R, Mark DF, Chamberlain K, Cohen BE, Vye-Brown C (2016) A 1 million year eruption history of Ascension Island: insights from stratigraphy and 40Ar/39Ar dating. In: Cities on volcanoes 9 Puerto Varas Chile November 2016

Preece KJ, Barclay J, Brown RJ, Chamberlain KJ, Mark DF (2021) Explosive felsic eruptions on ocean islands: a case study from Ascension Island (South Atlantic). J Volcanol Geotherm Res 416. https://doi.org/10.1016/j.jvolgeores.2021.107284

Rojas-Agramonte Y, Williams I, Arkus R, Kröner A, García-Casco A, Lázaro C, Buhre S, Wong J, Geng H, Morales Echevarría C, Jeffries T, Xie H, Mertz-Kraus R (2017) Ancient xenocrystic zircon in young volcanic rocks of the southern Lesser Antilles arc. Lithos: 228–252. https://doi.org/10.1016/j.lithos.2017.08.002

Rojas-Agramonte Y, Kaus BJ, Piccolo A, Williams IS, Gerdes A, Wong J, Xie HX, Buhre S, Toulkeridis T, Montero P, Garcia-Casco A (2022) Zircon dates long-lived plume dynamics in oceanic islands. Geochem Geophys Geosyst 23. https://doi.org/10.1029/2022gc010485

Sagan M, Heaman LM, Pearson DG, Luo Y, Stern RA (2020) Removal of continental lithosphere beneath the Canary archipelago revealed from a U-Pb age and Hf/O isotope study of modern sand detrital zircons. Lithos 362–363:105448. https://doi.org/10.1016/j.lithos.2020.105448

Sakata S, Hirakawa S, Iwano H, Danhara (2013) Correction of initial-disequilibrium on U–Th–Pb system for dating of young zircons. Abstracts Goldschmidt 2013 A2116

Scarrow JH, Schmitt AK, Barclay J, Horstwood MSA, Bloore AJ, Christopher TE (2021) Zircon as a tracer of plumbing processes in an active magmatic system: insights from mingled magmas of the 2010 dome collapse, Montserrat, Lesser Antilles Arc. Caribbean J Volcanol Geotherm Res 420:107390. https://doi.org/10.1016/j.jvolgeores.2021.107390

Scarrow JH, Chamberlain KJ, Montero P, Horstwood MSA, Kimura J-I, Tamura Y, Chang Q, Barclay J (2022) Zircon geochronological and geochemical insights into pluton building and volcanic-hypabyssal-plutonic connections: Oki-Dōzen, Sea of Japan—a complex intraplate alkaline volcano. Am Mineral 107:1545–1562. https://doi.org/10.2138/am-2021-7861

Scarrow JH, Schmitt AK, Danišík M, Chamberlain KJ, Davies BV, Rushton J, Brown RJ, Barclay J (2023) Zircon double-dating, trace element and O isotope analysis to decipher late Pleistocene explosive-effusive eruptions from a zoned ocean-island magma system. Ascension Island Quat Sci Rev 319:108304. https://doi.org/10.1016/j.quascirev.2023.108304

Schärer U (1984) The effect of initial 230 Th disequilibrium on young U Pb ages: the Makalu case. Himalaya Earth and Planetary Science Letters 67(2):191–204

Schmitt AK, Stockli DF, Hausback BP (2006) Eruption and magma crystallization ages of Las Tres Vírgenes (Baja California) constrained by combined $^{230}Th/^{238}U$ and (U–Th)/He dating of zircon. J Volcanol Geotherm Res 158:281–295. https://doi.org/10.1016/j.jvolgeores.2006.07.005

Schmitt AK, Sliwinski J, Caricchi L, Bachmann O, Riel N, Kaus BJP, Cisneros de León A, Cornet J, Friedrichs B, Lovera O, Sheldrake T, Weber G (2023) Zircon age spectra to quantify magma evolution. Geosphere 19(4):1006–1031. https://doi.org/10.1130/GES02563.1

Shane P, Storm S, Schmitt AK, Lindsay JM (2012) Timing and conditions of formation of granitoid clasts erupted in recent pyroclastic deposits from Tarawera Volcano (New Zealand). Lithos 140–141:1–10. https://doi.org/10.1016/j.lithos.2012.01.012

Sigurdsson H (1977) Generation of Icelandic rhyolites by melting of plagiogranites in the oceanic layer. Nature 269:25–28

Sturm A, Schmitt AK, Danišík M (2024) Updating the Eifel record: zircon double-dating of tephras from Wehr volcano (East Eifel Germany) as marker horizons for the European Pleistocene loess stratigraphy. Quat Sci Reviews 338:108810. https://doi.org/10.1016/j.quascirev.2024.108810

Trail D, Watson EB, Tailby ND (2012) Ce and Eu anomalies in zircon as proxies for the oxidation state of magmas. Geochim Cosmochim Acta 97:70–87. https://doi.org/10.1016/j.gca.2012.08.032

Troch J, Ellis BS, Schmitt AK, Bouvier AS, Bachmann O (2018) The dark side of zircon: textural, age, oxygen isotopic and trace element evidence of fluid saturation in the subvolcanic reservoir of the Island Park-Mount Jackson Rhyolite, Yellowstone (USA). Contrib Mineral Petrol 173:1–17. https://doi.org/10.1007/s00410-018-1481-2

Valley JW (2003) Oxygen isotopes in zircon. Rev Mineral Geochem 53:343–385. https://doi.org/10.2113/0530343

Watson EB, Harrison TM (1983) Zircon saturation revisited: temperature and composition effects in a variety of crustal magma types. Earth Planet Sci Lett 64:295–304. https://doi.org/10.1016/0012-821X(83)90211-X

Weaver B, Kar A, Davidson J, Colucci M (1996) Geochemical characteristics of volcanic rocks from Ascension Island, South Atlantic Ocean. Geothermics 25:449–470. https://doi.org/10.1016/0375-6505(96)00014-4

Weber G, Caricchi L, Arce JL, Schmitt AK (2020) Determining the current size and state of subvolcanic magma reservoirs. Nat Commun 11:5477. https://doi.org/10.1038/s41467-020-19084-2

Webster JD, Rebbert CR (2001) The geochemical signature of fluid-saturated magma determined from silicate melt inclusions in Ascension Island granite xenoliths. Geochim Cosmochim Acta 65(1):123–136. https://doi.org/10.1016/S0016-7037(00)00515-9

Wiesmaier S, Deegan FM, Troll VR, Carracedo JC, Chadwick JP, Chew DM (2011) Magma mixing in the 1100 AD Montaña Reventada composite lava flow, Tenerife, Canary Islands: interaction between rift zone and central volcano plumbing systems. Contrib Mineral Petrol 162(3):651–669. https://doi.org/10.1007/s00410-010-0596-x

Williams IS, Claesson S (1987) Isotopic evidence for the Precambrian provenance and Caledonian metamorphism of high grade paragneisses from the Seve Nappes, Scandinavian Caledonides. II: Ion microprobe zircon U-Th-Pb. Contrib Miner Petrol 97:205–217

Williams I, Rojas-Agramonte Y, Kröner A (2016) The deficiencies and excesses of the very young. Abstracts SHRIMP-Workshop 2016 Granada Spain

Xu Z, Zheng YF, Zhao ZF (2018) Zircon evidence for incorporation of terrigenous sediments into the magma source of continental basalts. Sci Rep 8(1):178. https://doi.org/10.1038/s41598-017-18549-7. Erratum in: Sci Rep 8(1):17473. https://doi.org/10.1038/s41598-018-35991-3

Zhong SH, Li SZ, Seltmann R, Lai ZQ, Zhou J (2021) The influence of fractionation of REE-enriched minerals on the zircon partition coefficients. Geosci Front 12(3):101094. https://doi.org/10.1016/j.gsf.2020.10.002

Zhu Y-S, Yang J-H, Sun J-F, Wang H (2017) Zircon Hf-O isotope evidence for recycled oceanic and continental crust in the sources of alkaline rocks. Geology 45:407–410. https://doi.org/10.1130/G38872.1